Linear signal processing methods and decay ratio estimation

6

Douter de tout ou tout croire, ce sont deux solutions également commodes qui l'une et l'autre nous dispensent de réfléchir.

Henri Poincaré, La Science et l'hypothèse (1908)

6.1 Classical spectral estimation: Fourier transform-based methods

6.1.1 The Fourier transform

The Fourier transform (FT) is the most important tool for spectral analysis of signals with a stationary behavior. This transform is defined by:

$$X(f) = \int_{-\infty}^{\infty} x(t) e^{-i2\pi ft} dt \tag{6.1}$$

The coefficients $X(f_0)$ obtained from Eq. (6.1) measure the resemblance level between the signal $x(t)$ and the monochromatic signal $\exp(2\pi f_0 t)$. These coefficients indicate the presence or absence of the frequency f_0 in the analyzed signal $x(t)$, that is, the *frequency content* or *spectrum* of the signal. The square magnitude $|X(f)|^2$ is called the power spectrum density (PSD) and indicates how the average power of the signal $x(t)$ is disseminated along frequency.

In recent applications largely dominated by digital signals, the FT (by definition a continuous function in both time and frequency) cannot be applied directly, but it is necessary to introduce its discrete counterpart, both in frequency and in time, leading to the so-called discrete Fourier transform (DFT) defined by:

$$X(k) = \sum_{n=0}^{N-1} x(n) \exp\left(-j\frac{2\pi nk}{N}\right) \quad k = 0, 1, \ldots, N-1 \tag{6.2}$$

where $x(n)$ is a discrete-time version of $x(t)$ of *only* N points of signal. This truncated, discrete-time version must satisfy the sampling theorem, that is, the chosen sampling frequency f_s in Hz must be at least twice the maximum (*important*) frequency of the signal spectrum. It is worth mentioning that $x(n)$ is an abbreviated expression of $x(nT_s)$ with $T_s = 1/f_s$ the sample period, with no loss of generality. Given that now we have a discrete-time signal, the original spectrum $X(f)$ becomes a periodic function of multiples of the sampling frequency f_s. If we normalize this periodic continuous spectrum by the sampling frequency, we have a periodic function, the period of which is an

Linear and Non-Linear Stability Analysis in Boiling Water Reactors. https://doi.org/10.1016/B978-0-08-102445-4.00006-0

integer multiple of 1. Then if we multiply by 2π, the spectrum is now in multiples of 2π rad/s. Taking now the same number of samples N, as in the time, of the periodic continuous spectrum, we obtain the expression in Eq. (6.2) in which $X(k)$ represents the discrete spectrum of $X(f)$ and the frequencies k (here just indicated as an integer index) are separated by $\Delta\omega = 2\pi/N$ rad/s (or $\Delta f = f_s/N$ Hz) from each other.

In 1965, Cooley and Tukey (Cooley & Tukey, 1965) introduced an *algorithm* that diminishes significantly the number of operations (complex multiplications and sums) in the calculation of the DFT. This algorithm is known as the fast Fourier transform (FFT) and is now the standard in obtaining the spectrum of a discrete signal due to its easy implementation and its low computational complexity.

The square magnitude of the Fourier transform for both cases, continuous and discrete, is also called the *periodogram*.

6.1.1.1 About spectral resolution…introducing windowing

The most important issue in the DFT implementation is about *spectral resolution*, which consists of *separation* between *frequencies* that are near each other. This issue is completely related to the fact that we now have only a finite number of samples instead of the whole sequence of the sampled signal. To understand this situation, we consider the continuous cosine of a specific oscillation frequency, shown in Fig. 6.1. Using the sampling theorem, we obtain a discrete-time signal $x(n)$, indicated by a stem plot in red in this same Fig. 6.1. It is clear that to compute the DFT (Eq. 6.2), it is necessary to have a finite number of samples of this discrete-time signal, resulting in a process called *windowing* in which the resulting signal is just the product of the original signal with a *rectangular window* of N points $w_N(n)$, that is, $x_w(n) = x(n)w_N(n)$, as shown in Fig. 6.1. This latter signal $x_w(n)$ is introduced in Eq. (6.2) to compute the same N points in frequency. However, instead of having the spectrum of the original discrete-time signal, we have the convolution between the spectrum of $x(n)$ and $w_N(n)$, that is, $X_w(f) = X(f) * W_N(f)$. Of course, this is a problem because instead of having a Dirac delta function at the oscillation frequency, we have a Dirichlet function (spectrum of the rectangular window), spreading the spectra around the cosine oscillation frequency.

The issue now becomes how to adequately separate two frequencies that are so close each other. This problem is shown in Fig. 6.2. Here, the sum of two discrete cosines of close oscillation frequencies is considered. The FT of this signal consists of two Dirac deltas placed at their corresponding frequencies (here only the spectra corresponding to positive frequencies are plotted, the Hermitian symmetry is considered). Two cases are plotted in Fig. 6.2. In the first one, the DFT is computed (by FFT) considering only 50 samples of the original signal, sampled to 20 Hz, while the second one uses 500 samples to compute the same DFT. The result is clear; the two frequencies in the first case cannot be separated due to the spectrum of the rectangular window.

However, in the second case, the two frequencies are clearly separated. In this latter case we can observe that the spectrum of the rectangular window is clearly placed in each oscillation frequency (as in first case of 50 samples), however, now the frequency

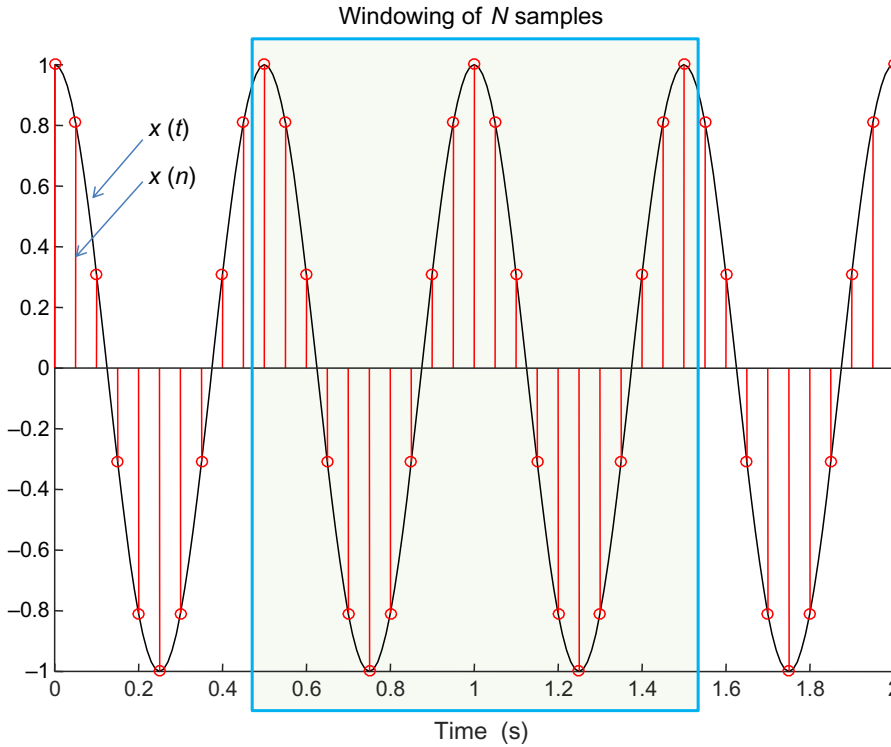

Fig. 6.1 The windowing issue.

spreading of the rectangular window is less, permitting us to observe both frequencies. This means that the resolution frequency depends, in an inverse way, of the number of samples N taken from the original signal. This is an important result to be considered when we are manipulating real signals, especially when we have only a small number of samples.

Based on these facts, some different functions (windows) were introduced to alleviate the frequency resolution problem. These windows try to diminish the effect of secondary (or side) lobes, presented in the spectrum of each of them, preserving only the spreading frequency effect of the principal lobe. This principal lobe is placed at the frequencies contained in the analyzed signal. A detailed panorama of different windows (in time and their respective spectra) is developed in Harris (1978). The most used windows are illustrated in Fig. 6.3. From this figure, we can establish a final remark about these windows: there is a tradeoff between the spreading of the principal lobe and the attenuation of the secondary lobes, that is, increasing the attenuation of secondary lobes lead to a major spreading of the principal lobe.

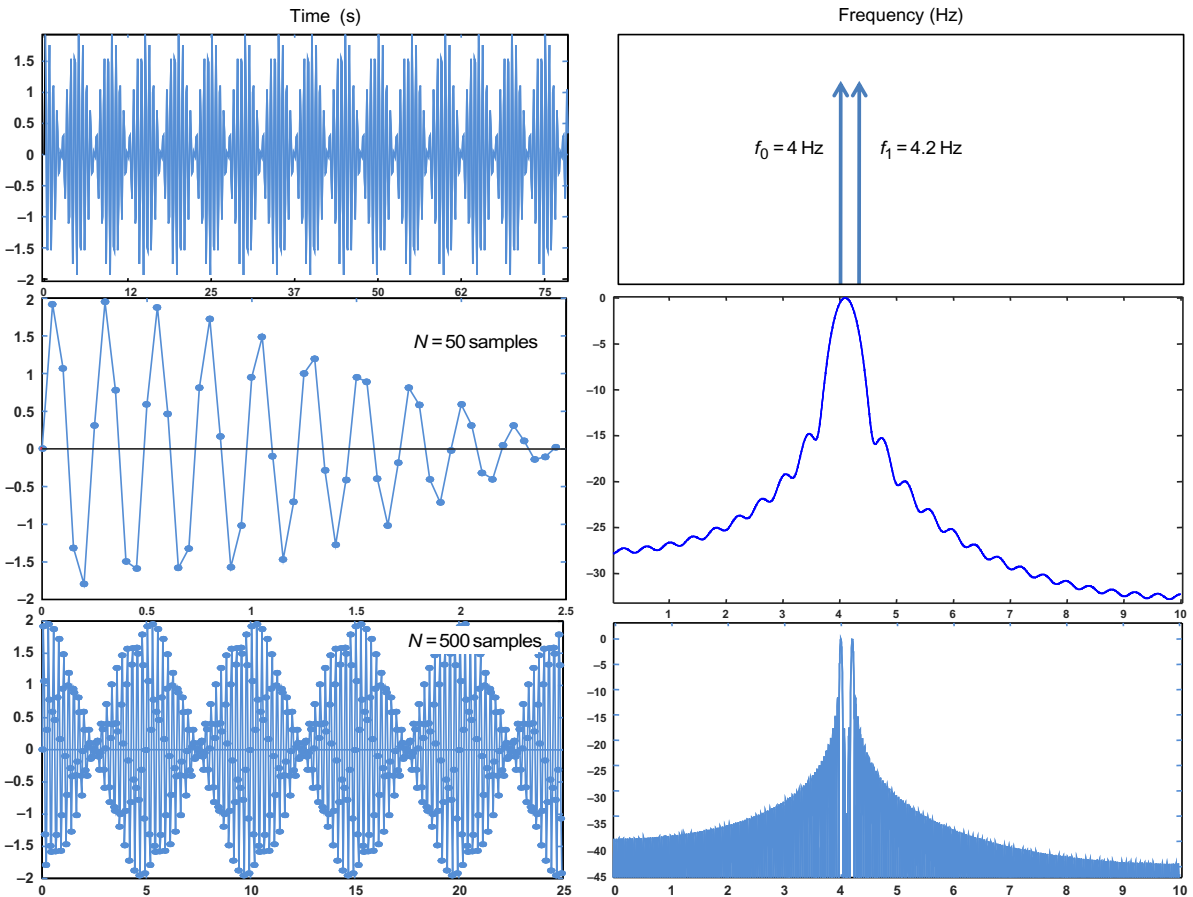

Fig. 6.2 The DFT resolution problem.

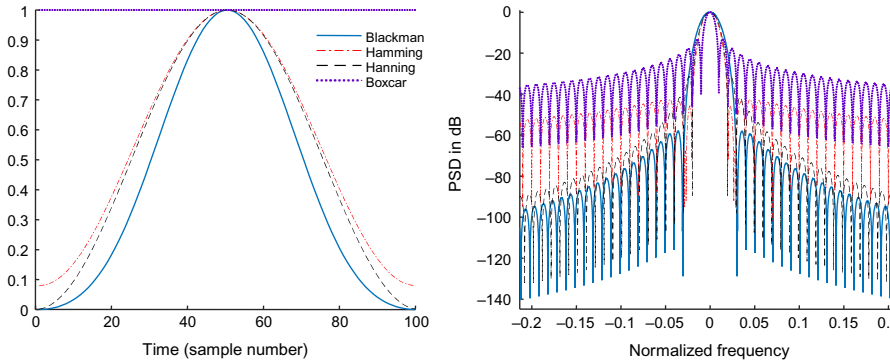

Fig. 6.3 Different practical windows.

6.1.2 Time-frequency representation: The short-time Fourier transform

Time-frequency analysis is an approach that describes the evolution of the information contained in the analyzed signal timewise. Time-frequency transformations compare the signal with a family of functions in which oscillations increase when the frequency under consideration increases, but the time support remains constant. Thus, the transformation is well adapted to signals oscillating in the neighborhood of well-defined frequencies.

6.1.2.1 Short-time Fourier transform

One of the most important time-frequency transformations is the short-time Fourier transform (STFT) introduced by Gabor in 1946 (Gabor, 1946). It uses windowing to analyze a small section of the signal in time, and it is defined by:

$$S(u,v) = \int_{-\infty}^{\infty} x(t) g^*_{u,v}(t) dt = \int_{-\infty}^{\infty} x(t) g(t-u) e^{-ivt} dt \tag{6.3}$$

where $x(t)$ is the signal to analyze and $g(t)$ is a window whose energy is concentrated in the neighborhood of u. This window measures the evolution in time of the spectral content of $x(t)$.

The Heisenberg's uncertainty principle establishes that the maximum resolution, in the time-frequency plane, is limited by the product $\sigma_t \sigma_\omega$ satisfying:

$$\sigma_t \sigma_\omega \geq \frac{1}{2} \tag{6.4}$$

where σ_t and σ_ω are the time and frequency spreads, respectively, of the *atoms* obtained by translations in time and frequency of the window g:

$$g_{u,v}(t) = g(t-u) e^{ivt} \tag{6.5}$$

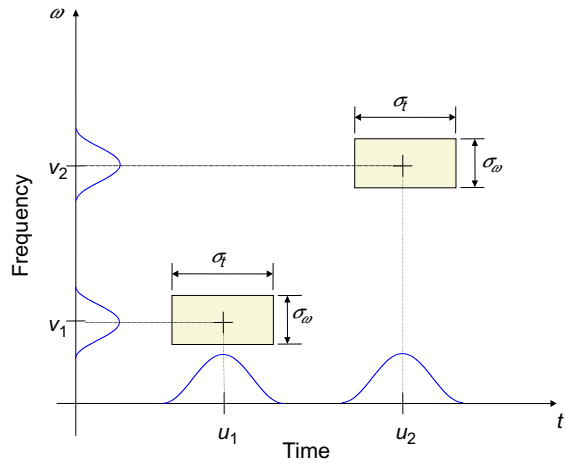

Fig. 6.4 Resolution of the time-frequency plane (STFT).

These *atoms* are shown in Fig. 6.4. It can be demonstrated that the product $\sigma_t \sigma_\omega$ remains constant and that is the same for the entire time-frequency plane. The maximum resolution is obtained with a Gaussian window, in which the atoms $g_{u,v}(t)$ are called Gabor functions.

The density of energy denoted as P_s is obtained by:

$$P_s = |S(u,v)|^2 = \left| \int_{-\infty}^{\infty} x(t) g(t-u) e^{ivt} dt \right|^2 \tag{6.6}$$

is called a *spectrogram* and measures the energy of the signal in the time-frequency neighborhood of (u, v).

Similar to the FT, the principal drawback of the STFT is that it depends on the chosen window$g_{u,v}(t)$, which is not well adapted to detect ruptures present in the signal. Based on this fact, the window choice is important, due to the fact that the FT of this window represents again its convolution in frequency with the spectrum of the analyzed signal. A rectangular window is not suitable for harmonic analysis when the frequencies in the analyzed signal are close to each other, as we discussed in the preceding section. Based on the results presented in Harris (1978), a good choice for this analysis may be a Hanning or a Hamming window (see Fig. 6.3). An overlap of 60% of these applied windows is used to avoid problems at the boundaries where the magnitudes of the data are attenuated due to the windowing.

In the next example, we consider a real instability event that occurred in a BWR, and that was described previously in Section 3.4. This BWR signal is shown in Fig. 6.5 together with its PSD obtained through the FFT. In this figure, we can observe the *global* frequency content of the signal, clearly showing an oscillation around 0.54 Hz and a possible harmonic around 1 Hz. However, we must be careful with the interpretation of these results. To understand why, we apply the STFT to the same BWR signal. The analysis is done using a Hanning window $g(t)$ with a percentage of

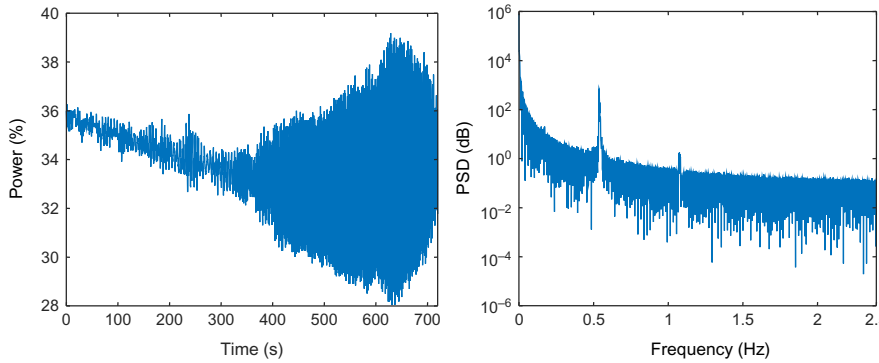

Fig. 6.5 A real stability event in a BWR and its PSD by FFT.

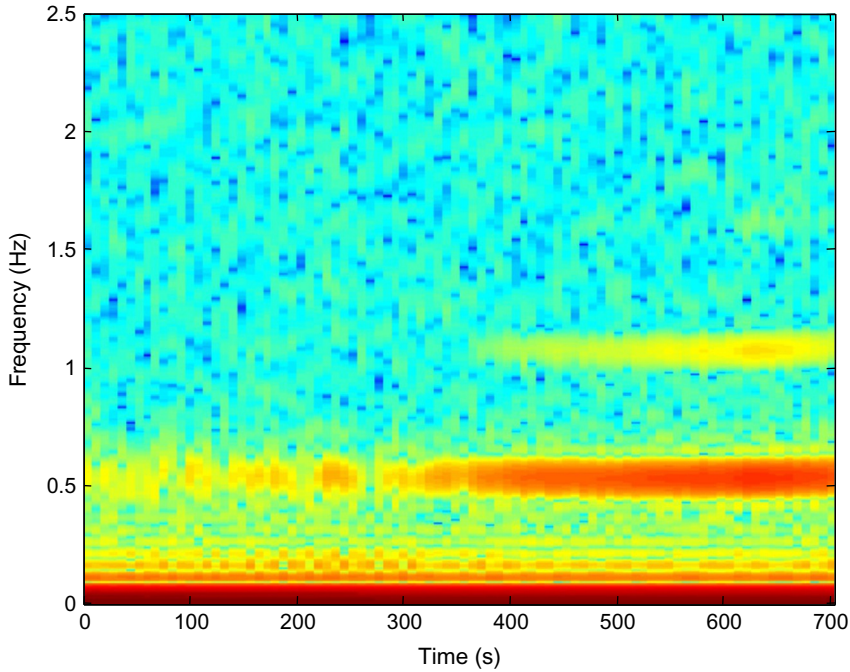

Fig. 6.6 The STFT of a real instability event in a BWR.

overlap of 60%, based on the recommendations presented in this section, and the number of signal samples N used in each window is 100 (20 s). In this interval, the BWR signal can be considered as stationary.

Results from the analysis are shown in Fig. 6.6. This figure shows the time-frequency plane (X-Y, respectively), where the darkest areas are the most important frequencies contained in the analyzed signal. As depicted in the figure, we can observe

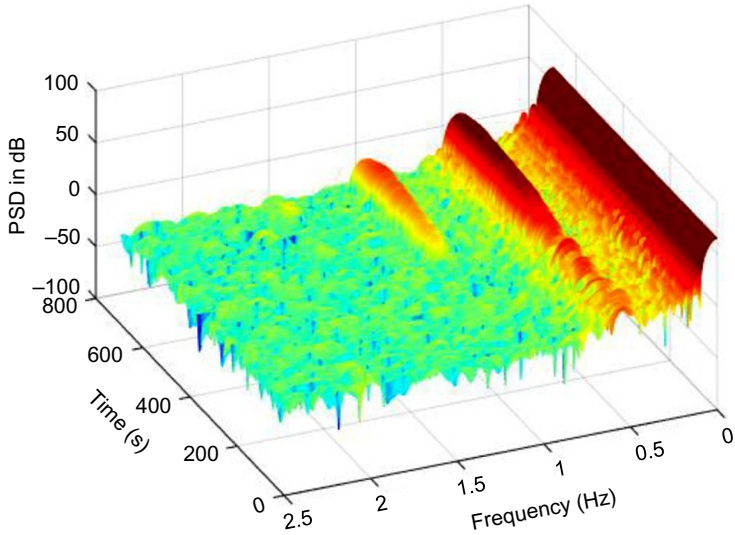

Fig. 6.7 Spectrogram in 3D of a real instability event in a BWR.

that the signal components have very low frequencies corresponding, in principle, to DC level (zero frequency) representing the signal trend. The instant in which the power level increases is marked by the frequency located in the neighborhood of 0.54 Hz. In this event, the frequency obtained from the measured data was (Farawila, Pruitt, Smith, Sánchez, & Fuentes, 1996) 0.54 Hz at 37% power rate and 37.8% flow rate, and 0.55 Hz at 33% power rate and 31.7% flow rate. This frequency is characteristic of the phenomenon known as a density-wave oscillation, explained previously in Section 3.3.4. Fig. 6.6 shows another frequency at 1.08 Hz that corresponds to a higher harmonic of the fundamental frequency of 0.5 Hz.

With this analysis we can perfectly determine the time evolution of frequencies contained in the analyzed signal. The global analysis considering only the Fourier transform does not permit us to *see* the frequency content evolution with the time of the signal. Besides the *stationarity* of the signal (as will be explained later) must be considered to validate the FT and show that the results are not misleading. This *frequency* evolution is more clearly shown in Fig. 6.7, in which the fundamental harmonic of the frequency at 0.54 Hz is presented and a higher harmonic around 1 Hz is more clearly observed.

6.1.3 The real world: The stochastic processes

Before presenting the most employed method to determine the stability indicator in BWRs, we need to introduce a powerful theory called *random or stochastic processes*, which we will apply to signals stemming, in general, from real physical phenomena.

A random process $X(t)$ can be defined as an *ensemble* of random variables that are functions of the time (in general, but not necessarily) in which a particular function

$x_i(t)$ of the ensemble is called a *realization* of the random process $X(t)$. Based on this definition, modeling an unpredictable signal (as practically all real signals are) by a stochastic process is to describe its temporal evolution by a multitude of functions of the variable time, in which each one of them is a possible realization of the phenomenon. The variable t can also be discrete, modeling a random phenomenon possibly issued from a sampling ($f_s = 1/T_s$), and represented by $X(nT_s)$ or simply $X(n)$. This latter process is sometimes called a *time series*. To illustrate and understand these concepts in a better way, we present in Fig. 6.8 some realizations stemming from a real phenomenon $X(t)$. Stochastic processes can be viewed in two ways:

- as a random variable constructed in a specific time t_0 over the whole ensemble of realizations and denoted by $X(t_0)$. At this specific time t_0 is defined the distribution $P_X(x(t_0))$ associated with this random variable. The moments (mean, variance, etc.) of this random variable can be obtained from the distribution. This procedure is repeated each time.
- as a random variable $x_i(t)$ obtained from each realization in an individual way along time. For this specific random variable, taken in this manner, a distribution $P_{X_i}(x_i)$ and its moments can be also established.

Unfortunately, many times in the real world it is not possible to have access to a sufficient number of realizations to characterize the process as an ensemble. Sometimes, we have only access to one realization of the random process, complicating its characterization more. However, there is a kind of process that fulfills a powerful property, *ergodicity*. This property relates the moments of the random variable $X(t_0)$ at each

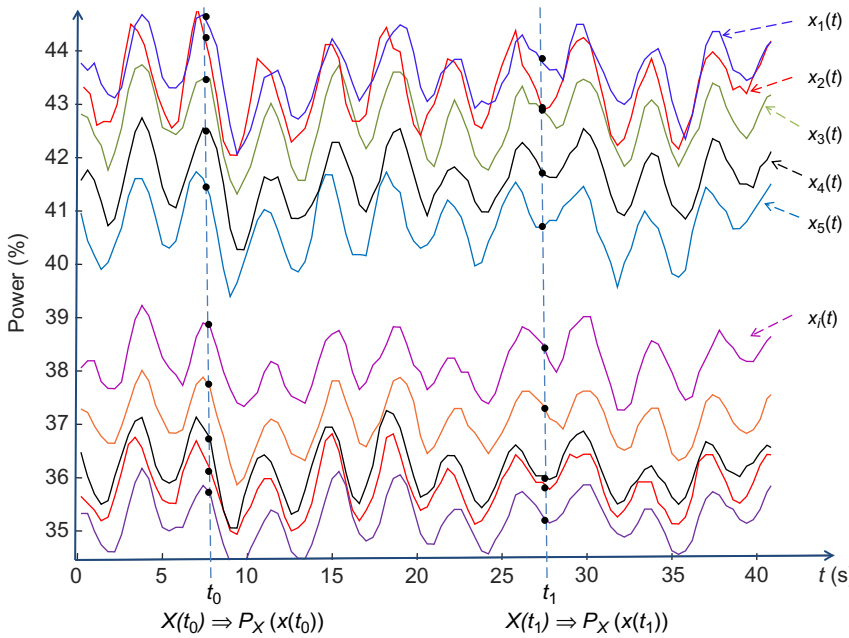

Fig. 6.8 Some realizations from a real random process.

specific time t_0, obtained over the ensemble of realizations, with the *temporal moments* obtained over each one of the realizations individually $x_i(t)$ and given by:

$$\int_{-\infty}^{\infty} [x_i(t)]^n dt = E[X^n(t)] \tag{6.7}$$

where $E[\cdot]$ is the mathematical expectation operator defined by:

$$E[X] = \int_{-\infty}^{\infty} x P_X(x) dx \tag{6.8}$$

It is clear that it is easier to obtain mean, variance, etc., directly from the integration of the signal representing a single realization of the stochastic process. However, for Eq. (6.7) to be fully satisfied, it is necessary that the moments, taken as a random variable over the complete process, be the same regardless of the time at which they are calculated. Of course, this is not a simple condition to satisfy in the real world. Because of this, we need to introduce another specific class of stochastic processes: *stationary processes in a wide sense*.

Definition 6.1. A process $X(t)$ is stationary in a wide sense if the two following conditions are fulfilled:

1. The mean of the process $m_X(t) = E[X(t)]$ is independent of t.
2. The autocorrelation function (ACF) $R_{XX}(t_1, t_2) = E[X(t_1)X(t_2)]$ depends only on the time difference $\tau = t_1 - t_2$ and not in an individual way, that is, $R_{XX}(\tau) = E[X(t)X(t-\tau)]$

To illustrate this concept, we consider again the realizations shown before in Fig. 6.8 and we introduce in Fig. 6.9 a possible autocorrelation function (bottom of figure) of this process under the assumption of stationarity in a wide sense. If we construct over the ensemble of realizations two different random variables at times t_1 and t_2, and we calculate the statistical correlation between these random variables, that is, $R_{XX}(t_1, t_2) = E[X(t_1)X(t_2)]$, it is unlikely (in real processes) to have the same result for this correlation independently of which time we consider. For this, the condition is relaxed to have only the same value of R_{XX} for the difference $\tau = t_1 - t_2$, as shown in Fig. 6.9. This seems more attached to reality, if we think that it is more likely to have a strong *statistical relationship* between two random variables close in time that stem from the same process. This *statistical relationship* in general diminishes when the time difference increases. Of course, sometimes this correlation value can be important again when the time difference increases, and can even be a periodic function (*cyclostationary process*). It is worth mentioning that the autocorrelation function is symmetrical around $\tau = 0$, that is, an even function $R_{XX}(\tau) = R_{XX}(-\tau)$. In this same figure, we also choose a specific realization to illustrate the concept of ergodicity, as was explained previously.

The autocorrelation function $R_{XX}(\tau)$, in addition to playing an important role in the complete description of the statistics of a stochastic stationary process, also links the

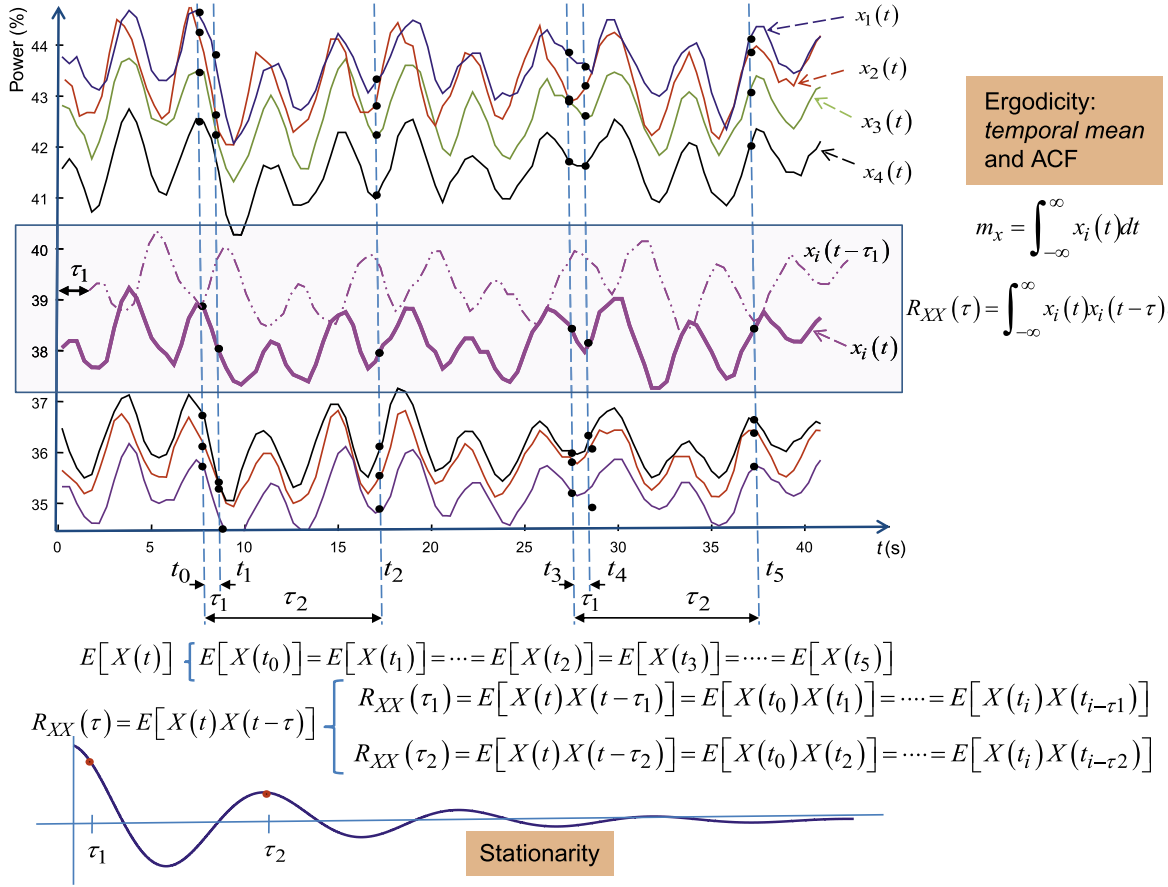

Fig. 6.9 Concepts of stationarity in a wide sense and ergodicity of a stochastic process.

average power of the process with its distribution along the frequency, through the so-called Wiener-Khinchin theorem (Khinchin, 1934):

$$S_{XX}(f) = \int_{-\infty}^{\infty} R_{XX}(\tau) e^{-j2\pi f\tau} d\tau \tag{6.9}$$

where $S_{XX}(f)$ is the power spectrum density (PSD) of the stationary process $X(t)$ and it is just the Fourier transform of the autocorrelation function of the process.

The problem again is that we have definitions considering the whole set of realizations. However, coupling the concept of *stationarity* and *ergodicity* (ergodicity implies stationarity but not the inverse), we can substitute the idea for a complete ensemble of realizations and handle a few of them, or even just one realization of the real process. Based on this relationship, we just need to be sure that our process is stationary in a wide sense and to force time averages to replace the statistics of the whole set. Thus, we only have to ensure that the first two time averages are the same during all the time of our realization(s), this is:

$$\begin{aligned} &E[X(t)] \quad \Rightarrow \quad m_X = \lim_{T\to\infty} \frac{1}{T} \int_{-T/2}^{T/2} x_i(t) dt \ \text{ and} \\ &R_{XX}(\tau) = E[X(t)X(t-\tau)] \ \Rightarrow \ R_{XX}(\tau) = \lim_{T\to\infty} \frac{1}{T} \int_{-T/2}^{T/2} x_i(t) x_i(t-\tau) dt \end{aligned} \tag{6.10}$$

From this last expression, we can deduce that in a practical implementation of the autocorrelation function, one can use estimators based on one or more realizations of the stochastic process. For example, for the case of a realization $x(n)$ of a sampled random process, the following unbiased estimator can be used:

$$\hat{R}_{XX}(k) = \frac{1}{N-k} \sum_{n=0}^{N-k-1} x(n) x(n-k) \tag{6.11}$$

for $k = 0, 1, \ldots, M$ where $M \leq N-1$ and N represents the *finite* number of samples of this realization. The estimated values of this function are called *lags*.

Based on the definition of DFT and the Wiener-Kinchin theorem, we can establish now the methods, direct and indirect, to obtain the power spectrum density for a real random process under the most important assumption: *stationarity*. These methods are shown in Fig. 6.10. We can observe that the direct method performs on the analyzed signal the Fourier transform (or its counterpart the DFT, based on the FFT) obtaining the square of this transformation to estimate the PSD directly. Meanwhile the indirect method estimates first the temporal autocorrelation function of the analyzed signal to determine, in a second step, this same PSD.

In either case, the direct or indirect method requires that the stationarity condition be satisfied in order to obtain (estimate) a reliable PSD. This condition is not usually fulfilled in the real world; therefore, it is necessary to introduce a third (heuristic)

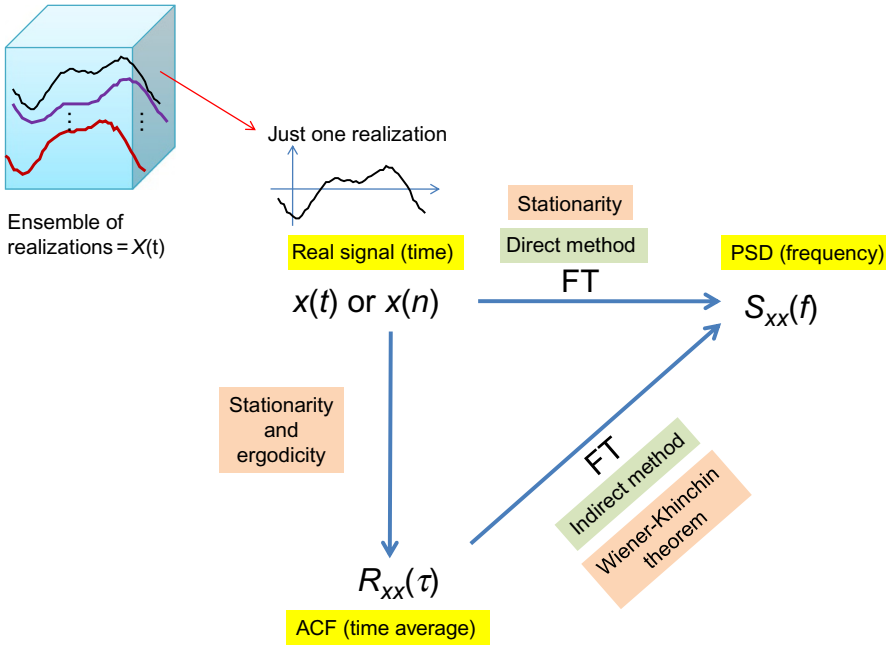

Fig. 6.10 Direct and indirect methods to obtain the power spectrum density of a real phenomenon.

option to estimate the PSD. This one considers a possible realization of the stochastic process and treats it in *small segments* as a square summable sequence (Priestley, 1981). For this, let $x_i(t)$ be any *typical* realization of the random process $X(t)$ of mean zero, then:

$$\frac{1}{N}\sum_{i=1}^{N} x_i^2(t) \approx \sigma_X^2 \equiv E\left[X^2(t)\right] \tag{6.12}$$

for large N. This point of view, considering the analysis by time segments of any realization of the random process, can also be linked with the idea of short-time Fourier transform presented before in Section 6.1.2. In this way, we have more reliable tools to estimate the spectral content of signals stemming from a real phenomenon.

6.2 Modern spectral estimation: Autoregressive model-based methods

Classical spectrum estimation makes no model assumption for the measurement signal and nowadays is based upon the use of the fast Fourier transform. Some windowed portion of the measurement is applied directly to the FFT, the output of which is used

to estimate the PSD. However, before the FFT algorithm, it was easier to obtain the PSD trough the indirect method (less complex operations of the DFT over the autocorrelation function instead the signal samples itself). In 1958, Blackman and Tukey (Blackman & Tukey, 1958) proposed a practical implementation for the PSD estimation from a discrete autocorrelation function estimated from windows of measured data. This method was practically the only one used to estimate the PSD, until the appearance of the FFT in 1965.

Modern spectrum estimation begins with the works of Burg in 1967 (Burg, 1967) and Parzen in 1968 (Parzen, 1968), introducing the maximum entropy method (MEM) and the autoregressive (AR) spectral estimation, respectively. Both methods are equivalents and they are based upon the assumption that the measurement signal is generated by a *prescribed model*, which is characterized by a number of parameters. Modern spectrum estimation, in general, can be viewed as a three-step methodology:

1. *A model selection* for the analyzed data.
2. *An estimation of model parameters* through algorithms performed directly on the measurements (data) or on the autocorrelation function (either estimated from the data or known).
3. *The PSD estimation*, inserting the estimated parameters directly into an analytical expression obtained from the model.

The selection of a model for the estimation of PSD allows us to give a *physical meaning* to it through an existing connection with the theory of linear systems.

6.2.1 The autoregressive model

The most popular linear model to estimate the PSD, even in our days, is the autoregressive model or simply the AR model. There are two points of view that allow establishing an AR model. The first one considers that the analyzed signal is the output of a system for which the input is unknown, while the second one considers that the analyzed signal can be estimated as a linear combination of past values of itself (more practical case). In both cases, and under certain conditions, the parameters of the AR model are the same. Based on these two points of view, the estimation of the parameters associated with this model can also be derived in two different ways. The first way is to carry out the estimate considering the orthogonality principle in stochastic processes, and the second, through a least-squares method. In the following paragraphs we will explain in detail this model and its parameter estimation from these two different points of view.

The AR model of a discrete signal $x(n)$ (our real signal) can be formulated as the resulting output of a system that is driven by the input $v(n)$ and linked through the next relation:

$$x(n) = -\sum_{k=1}^{p} a_k x(n-k) + v(n) \tag{6.13}$$

where p is the model order and a_k, $k = 1, 2, \ldots, p$, the AR model parameters. Here, $x(n)$ is a random process, stationary in a wide sense, and the input $v(n)$ is a Gaussian white

noise (a random process with a flat spectrum and a normal distribution $N(0,1)$). Rewriting Eq. (6.13):

$$v(n) = e(n) = x(n) + \sum_{k=1}^{p} a_k x(n-k) \tag{6.14}$$

Now the input of the system can be viewed as the difference $e(n)$ between the current value of $x(n)$ and a linear combination of its past values. This difference can also be treated as a Gaussian distributed error function.

Based on these considerations, we can apply the orthogonality principle to obtain parameters a_k. This principle establishes that the optimal estimation is obtained when the resultant error is orthogonal to the observations (measurements), that is:

$$E[e(n)x(m)] = 0 \quad m = 1,2,\ldots,p \tag{6.15}$$

Applying Eq. (6.15) to Eq. (6.14) and developing:

$$\begin{aligned} E[e(n)x(m)] &= E\left[\left(x(n) + \sum_{k=1}^{p} a_k x(n-k)\right)x(m)\right] = 0 \quad m = 1,2,\ldots,p \\ &= E[x(n)x(m)] + \sum_{k=1}^{p} a_k E[x(n-k)x(m)] \\ &= R_{xx}(m) + \sum_{k=1}^{p} a_k R_{xx}(m-k) = 0 \end{aligned} \tag{6.16}$$

then we have:

$$\sum_{k=1}^{p} a_k R_{xx}(m-k) = -R_{xx}(m) \quad m = 1,2,\ldots,p \tag{6.17}$$

where $R_{xx}(m)$ is the discrete autocorrelation function of the signal $x(n)$ which is an even function, $R_{xx}(-m) = R_{xx}(m)$ due to signal stationarity. The equations given in Eq. (6.17) are called the Yule-Walker equations (Yule, 1927; Walker, 1931) and they can be written in a matrix form:

$$\begin{bmatrix} R_{xx}(0) & R_{xx}(1) & R_{xx}(2) & \cdots & R_{xx}(p-1) \\ R_{xx}(1) & R_{xx}(0) & R_{xx}(1) & \cdots & R_{xx}(p-2) \\ R_{xx}(2) & R_{xx}(1) & R_{xx}(0) & \cdots & R_{xx}(p-3) \\ \vdots & \vdots & \vdots & \ddots & \vdots \\ R_{xx}(p-1) & R_{xx}(p-2) & R_{xx}(p-3) & \cdots & R_{xx}(0) \end{bmatrix} \begin{bmatrix} a_1 \\ a_2 \\ a_3 \\ \vdots \\ a_p \end{bmatrix} = - \begin{bmatrix} R_{xx}(1) \\ R_{xx}(2) \\ R_{xx}(3) \\ \vdots \\ R_{xx}(p) \end{bmatrix} \tag{6.18}$$

$$\mathbf{R}_{xx}\mathbf{a} = -\mathbf{r}_{xx}$$

From Eq. (6.18) we can observe that parameters a_k of the AR model can be obtained by inverting the matrix $\mathbf{R}_{xx}$. This matrix is known as the *correlation matrix* of the signal

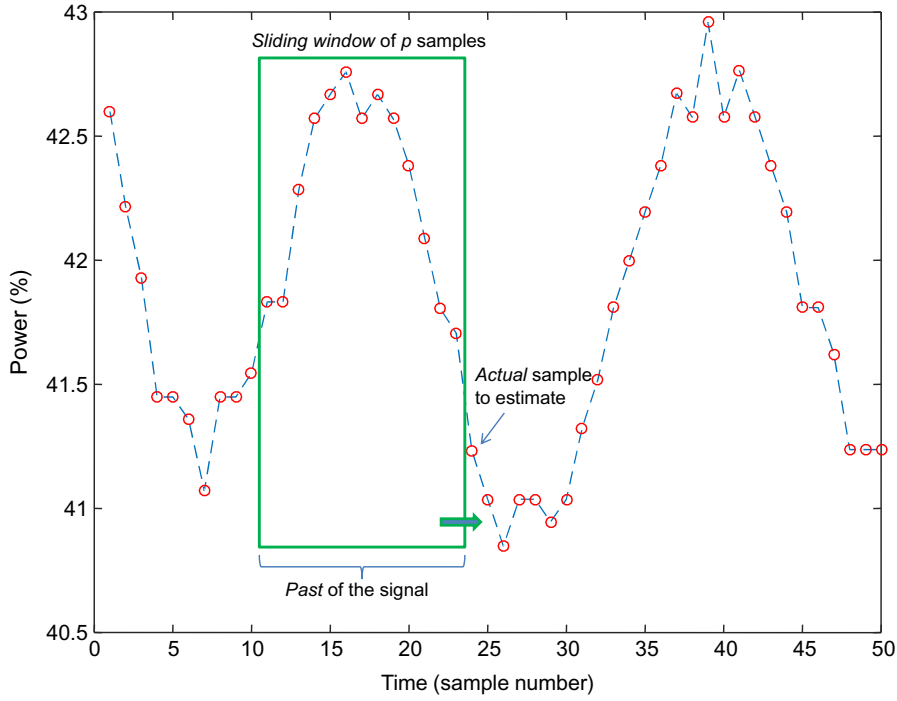

Fig. 6.11 A linear predictor of the signal $x(n)$.

$x(n)$. We also can observe that we only need the first $p + 1$ samples of the autocorrelation function $R_{xx}(n)$ to estimate the AR model parameters.

However, from a practical point of view, in many applications, the input $v(n)$ is not really known. In this case, the AR model established in Eq. (6.13) becomes simply a linear predictor that depends on a certain number of past samples of the signal $x(n)$. This linear combination to estimate the current sample of $x(n)$, based on its p last samples, and shown in Fig. 6.11, is given by:

$$\hat{x}(n) = -\sum_{k=1}^{p} a_k x(n-k) \tag{6.19}$$

This second point of view permits us to see the estimation at each time n as a sliding time window of size p, performing a linear weighted summation of the past samples of the signal. For this reason, this kind of predictor is called a Moving Average process or simply MA process.

Now, we are able to define an error function between the real signal $x(n)$ and its estimate $\hat{x}(n)$:

$$e(n) = x(n) - \hat{x}(n) = x(n) + \sum_{k=1}^{p} a_k x(n-k) \tag{6.20}$$

The best estimate $\hat{x}(n)$ is obtained minimizing the next criterion:

$$\frac{\partial}{\partial a_k}\left(E\left[e^2(n)\right]\right) = 0 \tag{6.21}$$

In this criterion, it is necessary to introduce the operator $E[\cdot]$ because the error (or residual) $e(n)$ is a random process like $x(n)$. Applying this criterion to Eq. (6.20), we obtain the same set of equations given in Eq. (6.18). In time series forecasting, this set of equations, obtained like a linear prediction, are also called the *normal equations* or the *Wiener-Hopf equations*, and the parameters a_k are called the linear prediction coefficients or simply the LPC.

The two points of view are similar in results; however, we must be prudent in their interpretation and use. The first case considers that the process is driven by a white Gaussian noise. The second one considers a sliding time window through the random process to estimate *the present* of this signal based on its own past. Both methods are exactly the same if the error function in Eq. (6.20) results with the linear prediction a white Gaussian noise. This means that for a stochastic process to be well modeled in an AR model, $e(n)$ must have a Kronecker delta autocorrelation function ($R_{ee}(k) = \delta(k)$) and must be Gaussian-distributed in amplitude. That is not always true for a real random process, as is shown in the next real example.

In this example, a vowel /i/ is the analyzed signal $x(n)$ (Fig. 6.12). It is well known that the speech signal is a random process, considered stationary in a wide sense only on small segments of 10–20 ms (practically a phoneme). Considering an order $p = 10$ (an also well-known parameter for this kind of process), we can obtain the LPC resolving equations given in Eq. (6.18).

Fig. 6.13 shows the resulting estimated signal $\hat{x}(n)$ and the model error $e(n)$. This same figure also displays the autocorrelation function and the distribution in amplitude (estimated by a histogram) of this model error.

Observing the residual signal in Fig. 6.13, we can conclude definitely that the random process (the vowel /i/ in this case) was not completely *whitened* by the AR model. Indeed, the residual shows some *peaks* in its autocorrelations function (giving a *periodic* appearance) and its amplitude distribution is not completely fitted by a Gaussian. This *periodicity* introduced in the autocorrelation function of the residual is called the *pitch* of the speaker. This problem, and the mechanisms that produce it, are well known in speech analysis.

For each stochastic process in question (including signals stemming from a BWR), we must be sure that the AR model complies with the signal *whitening* conditions, verified through the distribution and the autocorrelation function of the residue; to be used correctly later.

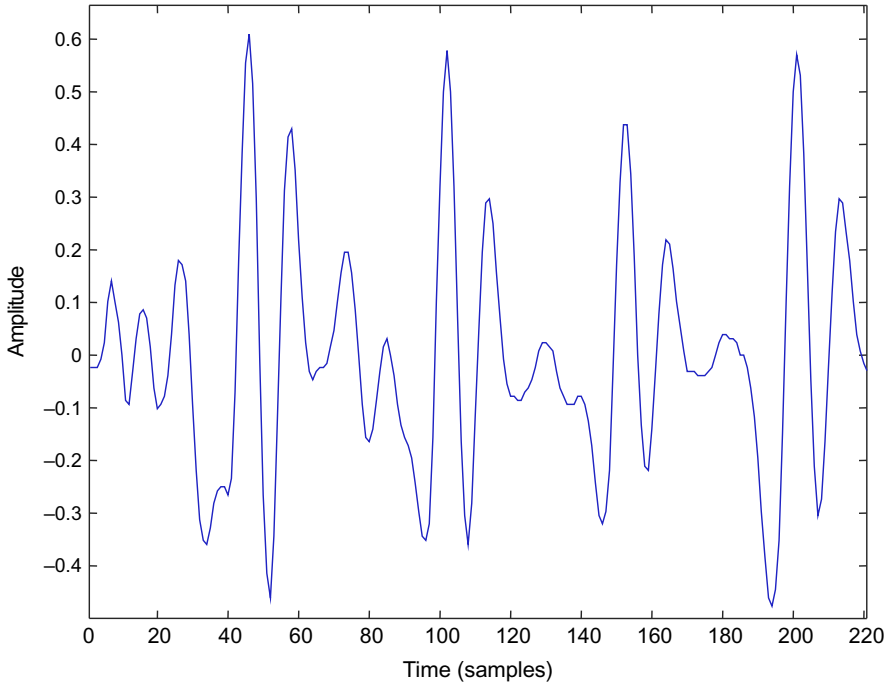

Fig. 6.12 A *realization* of the vowel /i/.

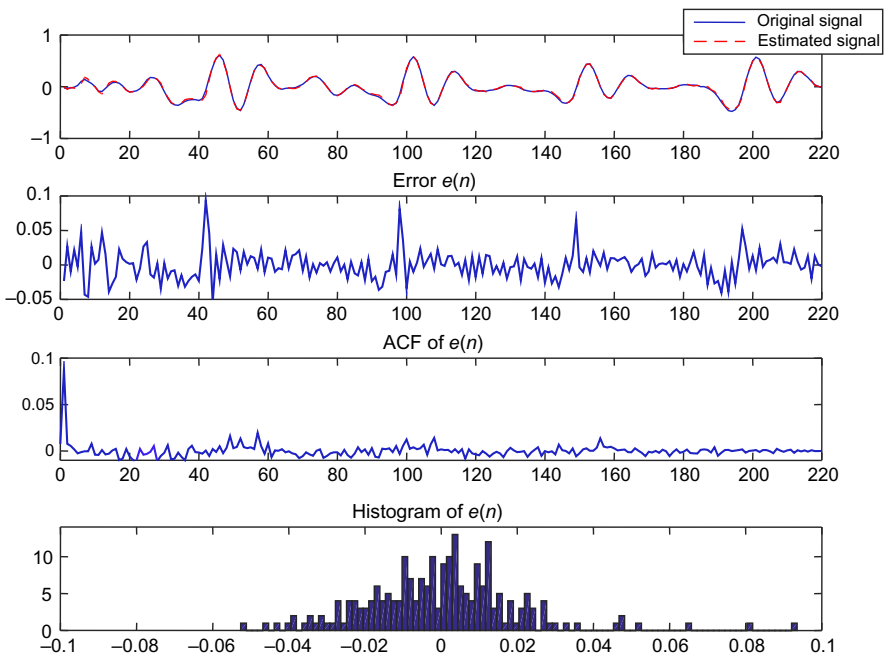

Fig. 6.13 The estimated signal and its residual (autocorrelation function and distribution) of the vowel /i/.

6.2.1.1 The Levinson-Durbin algorithm

Inverting the matrix $\mathbf{R}_{xx}$ to solve Eq. (6.18) can be a problem in real time implementations. Indeed, to obtain the LPC, we need to calculate the inverse of a possible large square matrix (10×10, in the last example). To alleviate this possible issue, Levinson (Levinson, 1947) proposed an algorithm in which the AR model parameters are obtained recursively. The Levinson's method was enhanced by Durbin (Durbin, 1960), doing it twice as fast. The steps of this iterative procedure, now called the Levinson-Durbin algorithm, are:

Step 1. Initialization.

$$a_{11} = \frac{-R_{xx}(1)}{R_{xx}(0)}$$
$$\sigma_1^2 = \left(1 - |a_{11}|^2\right) R_{xx}(0)$$

Step 2. Recursion for $k = 2, 3, \ldots, p$, given by:

$$a_{kk} = \frac{-\left[R_{xx}(k) + \sum_{l=1}^{k-1} a_{k-1,l} R_{xx}(k-1)\right]}{\sigma_{k-1}^2}$$
$$a_{ki} = a_{k-1,i} + a_{kk} a_{k-1,k-i}^*$$
$$\sigma_1^2 = \left(1 - |a_{kk}|^2\right) \sigma_{k-1}^2$$

In this way, the algorithm permits us to compute the parameter sets $\{a_{11}, \sigma_1^2\}$, $\{a_{21}, a_{22}, \sigma_2^2\}$, …, $\{a_{p1}, a_{p2}, \ldots, a_{pp}, \sigma_p^2\}$. This means that we compute an (intermediate) AR model of lower order fitting the same data. The coefficients a_{kk}, $k = 1, 2, \ldots, p$ in the recursion are called the reflection coefficients K_k, $k = 1, 2, \ldots, p$.

6.2.1.2 The order selection of the AR model

The classical order selections of the AR model are the final prediction error (FPE) and Akaike's information criterion (Akaike, 1969, 1973), the criterion autoregressive transfer function (CAT) (Marple, 1987), and the minimum description length (MDL) (Rissanen, 1978) given by:

$$FPE(p) = \frac{N+p}{N-p} \hat{\sigma}_e^2,$$
$$AIC(p) = N \log\left(\hat{\sigma}_e^2\right) + 2p,$$
$$CAT(p) = \frac{1}{N^2} \sum_{k=1}^{p} \frac{N-k}{\hat{\sigma}_e^2} - \frac{N-p}{N\hat{\sigma}_e^2},$$
$$MDL(p) = -\log\left(\hat{\sigma}_e^2\right) + \frac{1}{2} p \log(N),$$

where $\hat{\sigma}_e^2$ is the estimated variance (power) of the prediction error (the white Gaussian noise) at order p, considering N samples of the signal $x(n)$. The optimum order is considered as the minimum of each of these criteria.

6.2.2 PSD estimation based on the AR model

To link the AR model with the PSD of $x(n)$, we need to first calculate the z-transform of Eq. (6.14):

$$E(z) = \left[1 + \sum_{k=1}^{p} a_k z^{-k}\right] X(z) = A(z)X(z) \tag{6.22}$$

Hence, it is clear that the AR model can be seen as a system driven by a white Gaussian noise of power σ_e^2 as shown in Fig. 6.14.

From Eq. (6.22), we can obtain the transfer function of this AR model as:

$$H(z) = \frac{X(z)}{E(z)} = \frac{1}{A(z)} = \frac{1}{1 + \sum_{k=1}^{p} a_k z^{-k}} \tag{6.23}$$

Based on this result, the AR model is also called an *all-pole* model. Now, from Eq. (6.23), the PSD associated with process $x(n)$ can be estimated by evaluating this transfer function $H(z)$ in $z = e^{j\omega} = e^{j2\pi f}$ with the result:

$$\hat{S}_{xx}(f) = \left|H\left(e^{j2\pi f}\right)\right|^2 = \frac{\sigma_e^2}{\left|1 + \sum_{k=1}^{p} a_k e^{-j2\pi fk}\right|^2} \tag{6.24}$$

This PSD estimate $\hat{S}_{xx}(f)$ is called the *spectral envelope* of $x(n)$. Fig. 6.15 illustrates this concept through the PSD (based on Eq. 6.24) estimated from the LPC obtained from the speech example explained above.

It is important to mention that the PSD estimate $\hat{S}_{xx}(f)$ becomes the *true* $S_{xx}(f)$ when the order p of the AR model tends to infinity (Makhoul, 1975). This means that the autocorrelation function is taken into account in its totality (Wiener-Khinchin theorem) and not only the first $p+1$ samples.

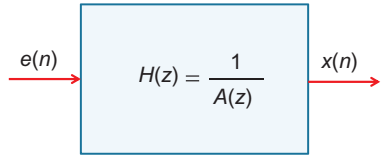

Fig. 6.14 The AR model viewed as a linear system.

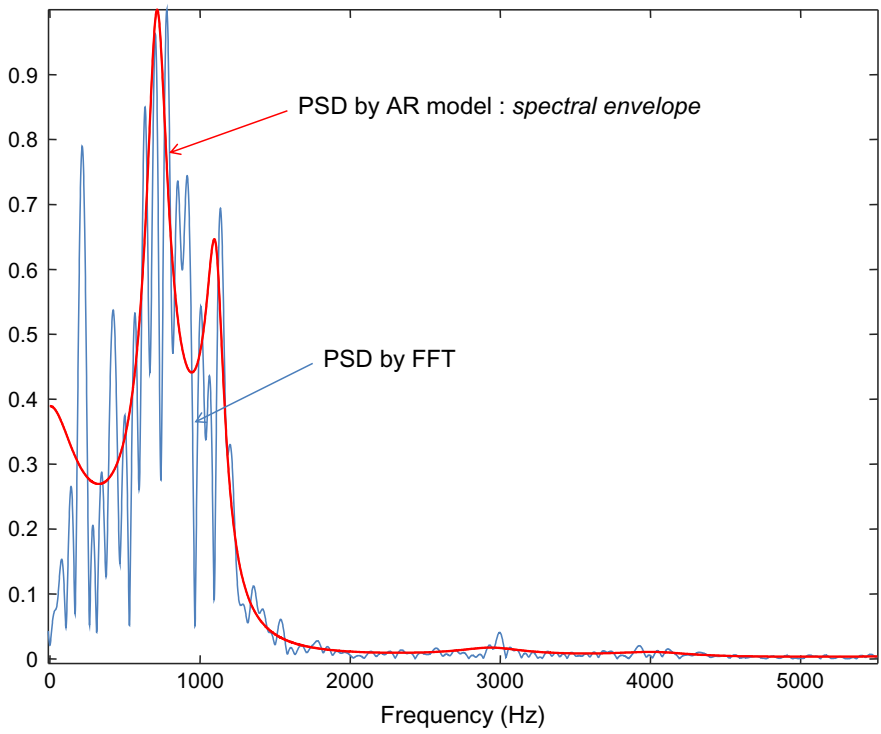

Fig. 6.15 The estimated PSD of the *realization* of the vowel /i/ based on an AR model.

6.3 Decay ratio estimation based on the FFT and AR models

Now that we have a linear model to fit a real random process, we can link this model with that used in the case of the BWR system (a second order linear model introduced previously in Section 5.9) to get the associated stability parameter.

6.3.1 *It's all about the autocorrelation function and power spectrum density!*

Before establishing the relationship between the stability parameter of a linear second-order system and the AR model, we perform the next analysis using the AR model. We consider in Eq. (6.13), the excitation in the model as an impulse (a Kronecker delta), that is, $v(n) = \delta(n)$:

$$h(n) = -\sum_{k=1}^{p} a_k h(n-k) + \delta(n) \tag{6.25}$$

where $x(n)=h(n)$ is the output of this model (the impulse response). Multiplying both sides of Eq. (6.25) by $h(n-i)$ and summing over all n, we obtain an estimation of the autocorrelation function of the impulse response:

$$\begin{aligned}\sum_{n=-\infty}^{\infty} h(n)h(n-i) &= \sum_{n=-\infty}^{\infty}\left[-\sum_{k=1}^{p} a_k h(n-k)h(n-i)+\delta(n)h(n-i)\right] \\ &= -\sum_{k=1}^{p} a_k \sum_{n=-\infty}^{\infty} h(n)h(n-(i-k)) + \sum_{n=-\infty}^{\infty}\delta(n)h(n-i) \qquad (6.26)\\ \hat{R}_{hh}(i) &= -\sum_{k=1}^{p} a_k \hat{R}_{hh}(i-k) + \sum_{n=-\infty}^{\infty}\delta(n)h(n-i)\end{aligned}$$

resulting in:

$$\hat{R}_{hh}(i)=\begin{cases}-\sum_{k=1}^{p} a_k \hat{R}_{hh}(i-k) & 1\le|i|<\infty \\ -\sum_{k=1}^{p} a_k \hat{R}_{hh}(k)+1 & i=0\end{cases} \qquad (6.27)$$

Makhoul (Makhoul, 1973) demonstrated that the first $p+1$ values of the autocorrelation function of the impulse response are identical to the corresponding first $p+1$ values of the autocorrelation function of the signal $x(n)$:

$$\hat{R}_{hh}(i)=R_{xx}(i), \quad i=0,1,2,\ldots,p \qquad (6.28)$$

Now, the AR model issue can be viewed as a linear filter $H(z)$ in which the autocorrelation function of its impulse response $h(n)$ must fit the first $p+1$ values of the autocorrelation function of the real random process. Based on these results, the link between the transfer function $H(z)$ obtained through an AR model with the stability parameter DR is straightforward: both impulse responses for the AR model (real signals from the BWR) and for the linear second-order damped oscillator (model for the BWR dynamics introduced in Chapter 5) must be the same. Hence, the possibilities of obtaining the decay ratio are numerous and represent many years of research about the linear stability of BWRs. In general, almost all of these solutions play with the PSD or the ACF, either through the AR model or the second-order harmonic oscillator model, going from a discrete to a continuous domain or vice versa. The following figure illustrates this connection between the two domains (Fig. 6.16).

The goal of this chapter is not to present exhaustively the variations for the DR estimation, but to show this classical methodology and its importance in the study of the stability of BWRs. In Table 6.1, we present some methods for the estimation of the DR that are linked to AR models and FT, including those reported in the Forsmark stability benchmark (Verdú et al., 2001).

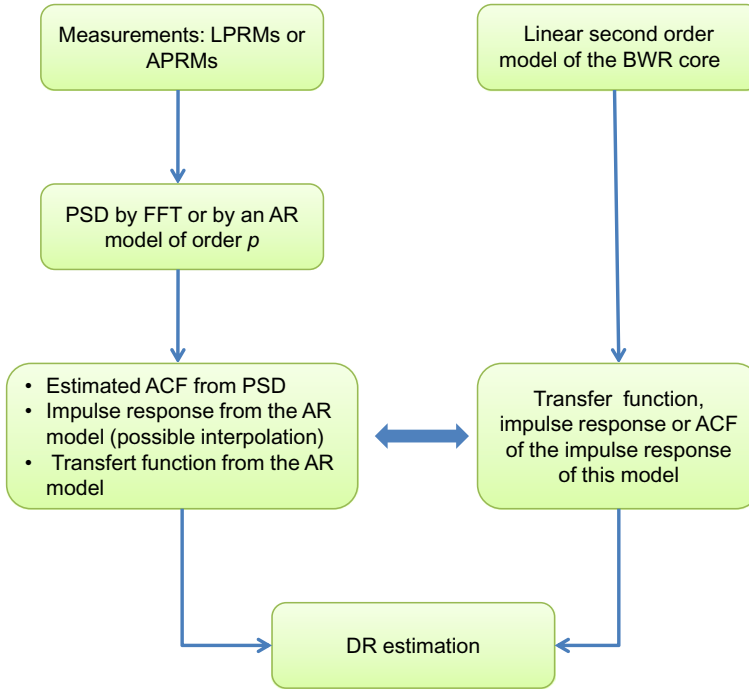

Fig. 6.16 The DR estimation issue.

Table 6.1 Some classical methods to estimate the DR

Method	Advantages	Disadvantages	Key references: DR estimation
Periodogram by FFT	• Output directly proportional to power. • Computationally efficient.	• Performance poor for short data segments. • Spectral resolution dependent on sample data. • Windowing distorts spectrum and masks weak signals.	Mitsutake, Tsunoyama, and Namba (1982)
Short-time Fourier transform	• Same as FFT. • Possible to apply to signals being stationary by time segments.	• Same as FFT. • Must consider overlapping of time windows.	Navarro-Esbrí, Ginestar, and Verdú (2003) and Espinosa-Paredes, Prieto-Guerrero, Núñez-Carrera, and Amador-García (2005)

Continued

Table 6.1 Continued

Method	Advantages	Disadvantages	Key references: DR estimation
AR, Yule-Walker	• Better resolution than FFT or BT. • No side lobes. • Model parameters linked to linear filtering.	• Model order must be selected. • Implied windowing distorts spectrum.	Forsmark stability benchmark
AR, Burg (maximum entropy)	• Same as AR-YW. • ACF interpolation (outside of the order p) implies no windowing.	• Model order must be selected. • Bias in the frequency estimates of peaks.	Forsmark stability benchmark
ARMA	• MA part enhances modeling.	• Model order of the MA and AR parts must be selected. • Computationally more complex than the AR model.	Forsmark stability benchmark

In Chapter 8, we will present in more detail the implementation of an algorithm based on the DR estimation considered as a monitoring system for the BWR core. Besides, we will include the problems related to the implementation of the AR model.

6.4 Wavelet-based methods and DR estimation

The work of Morlet and Grossmann (Goupillaud, Grossmann, & Morlet, 1984; Morlet, Arens, Fourgeau, & Giard, 1982) on reflection seismology introduces waveforms that are obtained by scaling a simple function that they call, in French, *ondelette* (wavelet). A wavelet ψ is a function of the time that satisfies the *admissibility condition*, which means that its *average value should be zero*, that is:

$$\int_{-\infty}^{\infty} \psi(t)dt = 0 \tag{6.29}$$

This function ψ, called the *mother wavelet*, is dilated by the scale parameter a, and translated in time by b. These scalings and translations produce a collection (family) of functions denoted by:

$$\psi_{a,b}(t) = \frac{1}{\sqrt{a}}\psi\left(\frac{t-b}{a}\right) \tag{6.30}$$

6.4.1 The continuous wavelet transform

The continuous wavelet transform (CWT) is obtained by computing the correlation (resemblance) between the signal $x(t)$ and these scaled and translated functions $\psi_{a,b}(t)$:

$$CWT_x(a,b) = \int_{-\infty}^{\infty} x(t)\psi^*_{a,b}(t)dt = \frac{1}{\sqrt{a}}\int_{-\infty}^{\infty} x(t)\psi^*\left(\frac{t-b}{a}\right)dt \tag{6.31}$$

Like the STFT, the CWT allows us to measure variations in time of spectral components, but the main difference resides in its resolution, which permits us to do a well-adapted analysis of signals with nonstationary features. The *atoms* obtained with the CWT are centered in time and frequency in b and (η/a), respectively. These *atoms* are shown in Fig. 6.17.

Fig. 6.17 shows the most important advantage of CWT: detection in time of well-located ruptures. When the scale a is small enough, the resemblance between the analyzed signal (e.g., a rupture) and the wavelet becomes relevant. Another important remark is that the scale a is inversely proportional to the frequency. It means that resolution must be sacrificed in frequency in favor of a better detection in time. In practice, ruptures are detected by the direct analysis of the coefficients $CWT_x(a,b)$ in the time-scale plane, determined by different values of a and b.

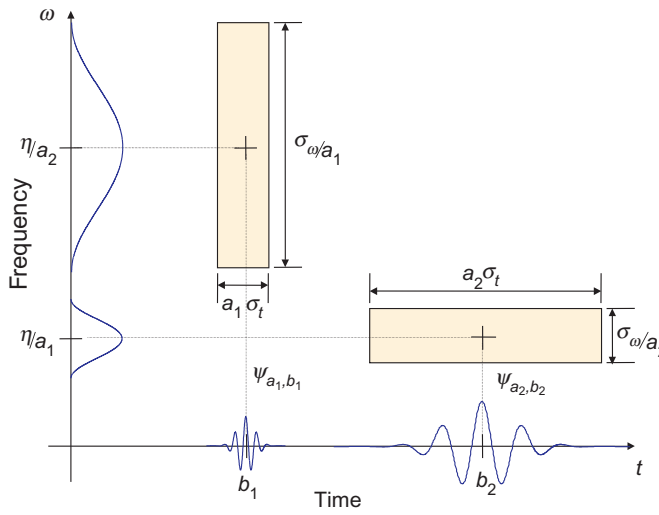

Fig. 6.17 Resolution of the time-scale plane.

The measured energy of each wavelet $\psi_{a,b}(t)$ can be represented, like the STFT, as a density of energy defined by:

$$S_W(a,b) = |CWT(a,b)|^2 \tag{6.32}$$

This density of energy is called a *scalogram*.

The time-scale plane represents an alternative domain for the analysis of the BWR signals. We illustrate this utilization with the instability signal used in the analysis with STFT. For this analysis we apply a mother wavelet Coiflet 2, shown in Fig. 6.18, in the Continuous Wavelet Transform. This wavelet exhibits important features, such as compact support and regularity.

In Fig. 6.19, we can see the evolution in time of the signal, but the principal difference between the preceding analysis with the time-frequency plane resides in the fact that the scale is not exactly the frequency (although they are related). Nevertheless, we can see in this figure the growing correlation between the signal and the mother wavelet at the instant in which the instability increases in the analyzed signal. Thus, we can say that the time-scale analysis represents a real alternative for the time-frequency plane.

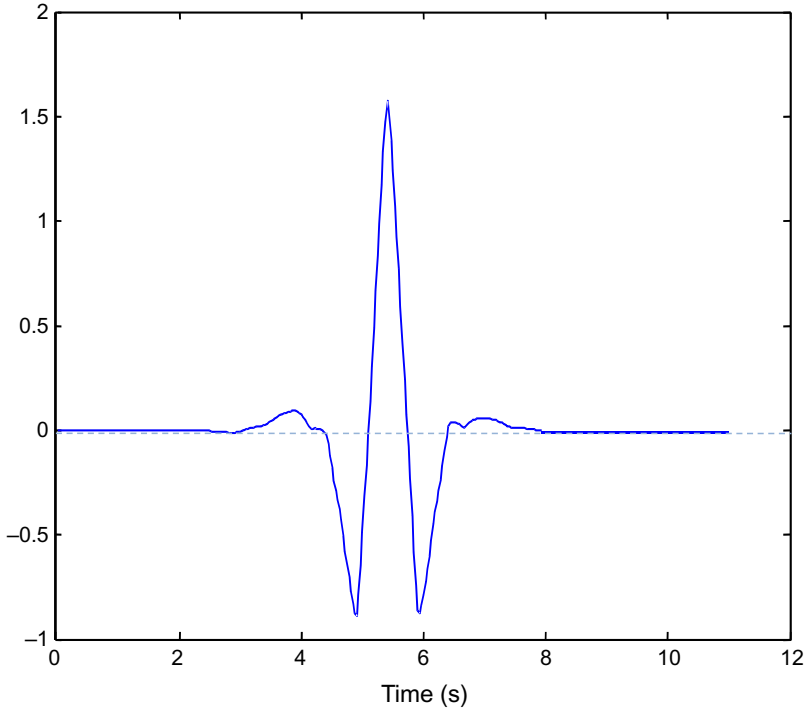

Fig. 6.18 The Coiflet 2 wavelet.

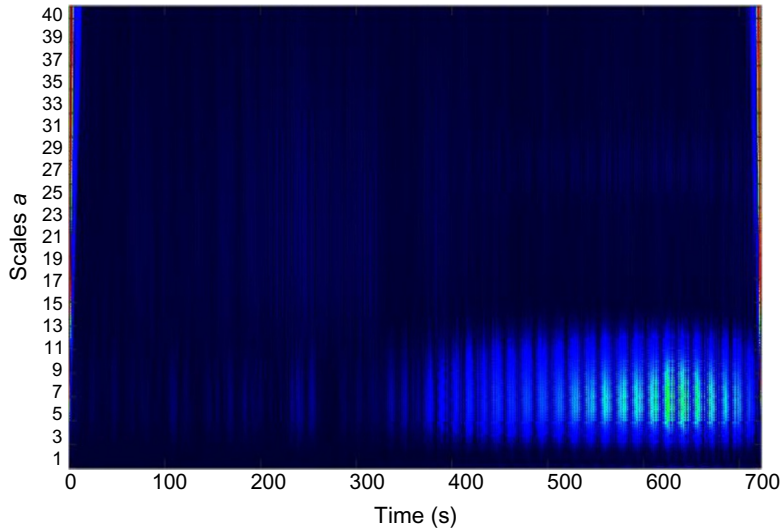

Fig. 6.19 CWT of a real BWR instability event.

An easier comprehension of this result is obtained if we introduce a relationship between the *frequency* and the *scale*. From the point of view of linear filtering, the CWT can be written as a convolution integral:

$$CWT_x(a,b) = \int_{-\infty}^{\infty} x(t)\psi^*\left(\frac{t-b}{a}\right)dt = x(\tau) * \left[\frac{1}{\sqrt{a}}\psi\left(\frac{-t}{a}\right)\right] \tag{6.33}$$

Obtaining the Fourier transform (FT):

$$\mathbf{CWT}_x(f) = X(f)FT\left[\frac{1}{\sqrt{a}}\psi\left(\frac{-t}{a}\right)\right] = X(f)\left[\sqrt{a}\hat{\Psi}^*(af)\right] \tag{6.34}$$

and considering the admissibility condition in Eq. (6.29), $\hat{\Psi}$ can be viewed as the frequency response of a band-pass filter, as shown in Fig. 6.20. This filter is centered and a precise frequency f_c that depends on the number of oscillations of each wavelet permits us to establish the next relationship between the scale and the frequency:

$$f_a = \frac{f_c f_s}{a} \tag{6.35}$$

where f_a represents the *pseudo frequency* (in Hz) linked to scale a (the approximated frequency at scale a), f_c is the central frequency (in Hz) of the wavelet used and f_s (in Hz) is the sampling rate of the analyzed signal.

Based on Eq. (6.35) of the example presented in Fig. 6.19, we can *approximately* determine the frequency corresponding to the maximum correlation (around scale 7)

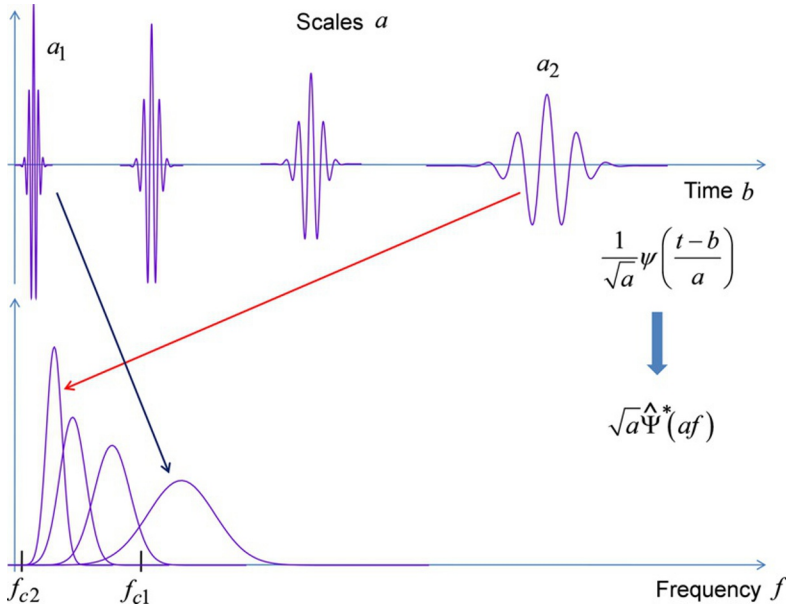

Fig. 6.20 Link between the *frequency* and the *scale*.

obtained in the time-scale plane. In this case, this frequency is *around* 0.52 Hz, similar to that obtained previously with the time-frequency analysis.

6.4.2 The wavelet ridges and the instantaneous frequency

A complex (or analytic) wavelet is a function whose spectrum has only positive frequencies. Because a complex wavelet only responds to the nonnegative frequencies of a given signal, it produces a transform whose modulus is less oscillatory than in the case of a real wavelet. This property is a real advantage in detecting and tracking instantaneous frequencies contained in the signal. In the next paragraphs, we will demonstrate the utility of complex wavelets to analyze signals obtained from a BWR. There exist some well-known families of complex wavelets. Among these functions, we can mention the complex Cauchy wavelet, the complex Mexican Hat wavelet, and the complex Morlet wavelet. In this book, we focus on the use of the Morlet wavelet for the estimation of the DR from BWR signals.

The complex Morlet wavelet is a complex sinusoid modulated by a Gaussian envelope defined by:

$$\psi(t) = \frac{1}{\sqrt[4]{\pi}} e^{j\omega_c t} e^{-\frac{t^2}{2}} \tag{6.36}$$

where $\omega_c = 2\pi f_c$ is the central frequency of the wavelet and determines the number of oscillations of the complex sinusoid inside the Gaussian envelope. To assure that the

expression in Eq. (6.36) is (*almost*) a wavelet, that is, a zero-mean function, the central frequency ω_c must be greater than 5. The term $1/\sqrt[4]{\pi}$ ensures that the wavelet has unit energy. The Fourier transform of the complex Morlet wavelet is given by:

$$\hat{\Psi}(\omega) = \sqrt{2}\sqrt[4]{\pi}\mathrm{e}^{-\frac{(\omega-\omega_c)^2}{2}} \tag{6.37}$$

and hence its energy spectrum is

$$\left|\hat{\Psi}(\omega)\right|^2 = 2\sqrt{\pi}e^{-(\omega-\omega_0)^2} \tag{6.38}$$

From Eqs. (6.33), (6.34), we can express the CWT as a product in the Fourier domain:

$$CWT_x(a,b) = \frac{1}{2\pi}\int_{-\infty}^{\infty} X(\omega)\hat{\Psi}^*_{a,b}(\omega)d\omega \tag{6.39}$$

where $X(\omega)$ is the Fourier transform of the analyzed signal $x(t)$ and

$$\hat{\Psi}^*_{a,b} = \sqrt{a}\hat{\Psi}^*(a\omega)e^{j\omega b} \tag{6.40}$$

is the Fourier transform of the mother wavelet at scale a and time b. When the Fourier transform of the wavelet is sharply concentrated at a fixed value of frequency, the CWT will have the tendency to *concentrate* at the frequency values associated with dominant harmonics in the signal, defining a series of curves called *ridges* that evolve along time. These ridges are locations at which the frequency of the scaled wavelet coincides with the local frequency of the signal, as will be demonstrated in the following paragraphs. The ridges theory can be established as follows, considering the analytic representation of a signal given by:

$$Z_x(t) \triangleq x(t) + j\hat{x}(t) = A(t)e^{j\phi(t)} \tag{6.41}$$

where $\hat{x}(t)$ is the Hilbert transform of the signal $x(t)$, which is defined as:

$$\begin{aligned}\hat{x}(t) &= x(t) * \frac{1}{\pi t} \\ &= \frac{1}{\pi}\int_{-\infty}^{\infty}\frac{x(\tau)}{t-\tau}d\tau\end{aligned} \tag{6.42}$$

$A(t)$ and $\phi(t)$ are the envelope and the instantaneous phase of the signal, respectively. This complex signal is completely characterized by the amplitude $A(t)$ and the phase $\phi(t)$ with values in the interval $[0, 2\pi)$, forming the so-called *canonical pair*. Because $\mathrm{Re}[Z_x(t)] = x(t)$:

$$x(t) = A(t)\cos(\phi(t)) \tag{6.43}$$

yielding the *canonical representation* of $x(t)$. It is clear that the analytic signal $Z_x(t)$ associated with $x(t)$ has the same amplitude and frequency range as $x(t)$; it also comprises the phase information of the original signal $x(t)$ and can be used to compute the instantaneous amplitude and to analyze the frequency performance of $x(t)$. For this, we suppose that the amplitudes from the signal and the wavelet are varying slowly, that is, these signals are considered asymptotic. From Eq. (6.41), the *instantaneous frequency*, in rad/s, is defined by:

$$\omega_{inst}(t) = \frac{d\phi(t)}{dt} \tag{6.44}$$

or in Hz

$$f_{inst} = \frac{1}{2\pi}\frac{d\phi(t)}{dt} \tag{6.45}$$

Considering now an analytic wavelet $\psi(t)$, also asymptotic, in a general form given by $\psi(t) = A_\psi(t)e^{j\phi_\psi(t)}$, the CWT of the signal $x(t)$ is then obtained by (Delprat et al., 1992):

$$CWT_x(a,b) = \frac{1}{2a}\int_{-\infty}^{\infty} A(t)A_\psi\left(\frac{t-b}{a}\right)\exp\left(j\left(\phi(t) - \phi_\psi\left(\frac{t-b}{a}\right)\right)\right)dt \tag{6.46}$$

Because the integrand is asymptotic, the stationary phase theorem given by Delprat (Delprat et al., 1992) can be applied. Let $\Phi_{a,b}(t) \triangleq \phi(t) - \phi_\psi((t-b)/a)$ be the argument of the integrand of Eq. (6.46) and $t = t_0$ be the stationary point of this argument, then:

$$\Phi'_{a,b}(t_0) = \phi'(t_0) - \frac{1}{a}\phi'_\psi\left(\frac{t_0-b}{a}\right) = 0 \tag{6.47}$$

$$\Phi''_{a,b}(t_0) = \phi''(t_0) - \frac{1}{a}\phi''_\psi\left(\frac{t_0-b}{a}\right) \neq 0 \tag{6.48}$$

Therefore the *ridge* of the CWT of $x(t)$ is the set of points (a,b), which are the stationary points of the argument $\Phi_{a,b}(t)$ in Eq. (6.47) (i.e., $(t_0(a,b) = b)$). The ridge can be calculated from Eq. (6.47) as:

$$a(b) = \frac{\phi'_\psi(0)}{\phi'(b)} \tag{6.49}$$

and the instantaneous frequency along this ridge becomes:

$$\omega_{inst}(t)|_{t=b} = \phi'(b) = \frac{\phi'_\psi(0)}{a(b)} \tag{6.50}$$

From Eqs. (6.49), (6.50), it is clear that the ridge is proportional to the instantaneous frequency and the latter must be calculated after the ridge extraction. Todorovska (Todorovska, 2001) has obtained an approximation for the CWT given by:

$$CWT_x(a,b) \approx \sqrt{\frac{\pi}{2}} \frac{Z_x(t_0)\psi^*\left(\dfrac{t_0-b}{a}\right)}{\text{corr}(a,b)} \tag{6.51}$$

where

$$\text{corr}(a,b) = a\left|\Phi''_{a,b}(t_0)\right|^{1/2} e^{-j(\pi/4)\,\text{sgn}\left[\Phi''_{a,b}(t_0)\right]} \tag{6.52}$$

For the case of the complex Morlet wavelet, at $t_0 = b$ this translated and dilated wavelet in Eq. (6.51) has its maximum, then at this same instant, the CWT is also locally maximum, neglecting the correction term $\text{corr}(a,b)$. This assumption gives a simple form to obtain the ridges from the local *maxima* of the amplitude of the CWT. The ridge concept is shown, in a simplified form, in Fig. 6.21. In this figure, a ridge point, associated with the time b, is indicated. This point represents the maximum of the signal at this instant of time. The respective scale a is also marked. At the bottom of Fig. 6.21, the conversion of this scale to the respective frequency is illustrated. This mapping is repeated for each estimated ridge point, giving the instantaneous frequency along time.

Based on these facts, using the *scalogram*, it is possible to obtain information about the *instantaneous frequencies* of the signal through the wavelet *ridges*, which are

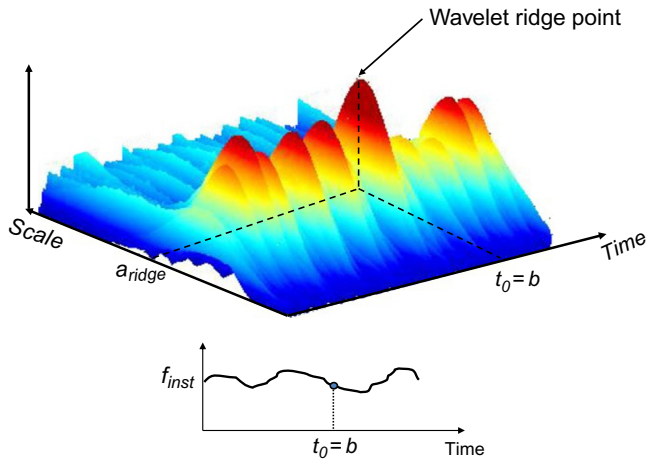

Fig. 6.21 Simplified representation for the wavelet ridges.

curves in the time domain following the maximum values of the normalized scalogram given by:

$$CWT_x\left(a_{ridge}, b = t_0\right) = \max\left[\frac{S_W(a,b)}{a}\right] \tag{6.53}$$

The corresponding instantaneous frequency at time t_0 is simply obtained according to:

$$f_{inst} = \frac{C}{a_{ridge}} \tag{6.54}$$

where C is a constant that depends directly on the mother wavelet used. Mallat (Mallat, 1998) also demonstrated that if the signal has multiple separable components (sum of different amplitudes and phases), it is possible to determine perfectly each instantaneous angular frequency.

We will repeat the CWT analysis of the signal representing a real instability event, but now using the complex Morlet wavelet defined before in Eq. (6.36). Generally, the parameter ω_0 is chosen to be larger than 5 to ensure that the integral of $\psi(t)$ is small enough (admissibility condition). Using the relationship between the scale and the frequency given by Eq. (6.35) with a sampling frequency of the signal of 5 Hz and $f_c = 2$ ($\omega_0 = 12.57$), we can approximately determine the frequency corresponding to the maximum correlation obtained in the time-scale plane, as illustrated in Fig. 6.22.

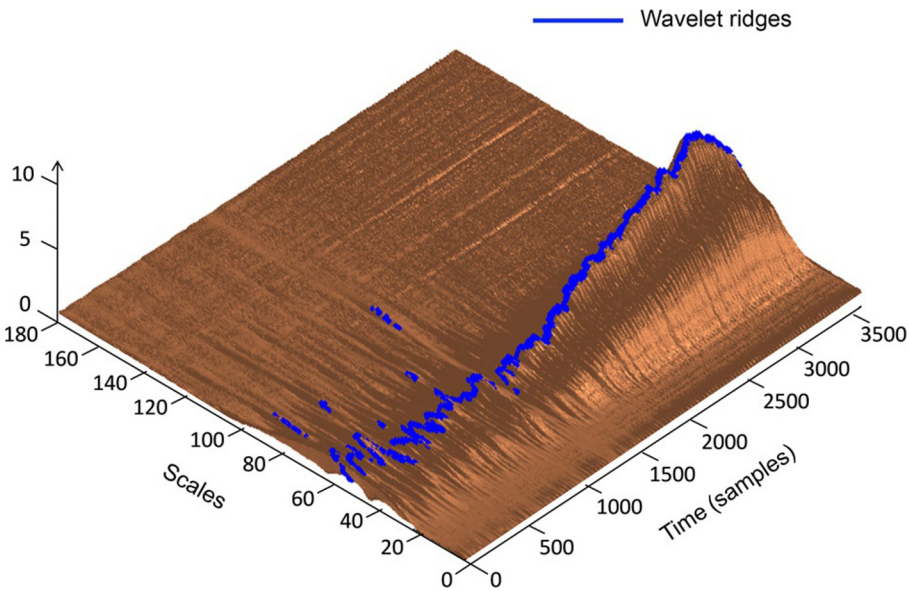

Fig. 6.22 Modulus maxima of the CWT and the wavelet ridges of a real instability event in a BWR.

In order to get a better appreciation of the results, as in the case of the ideal signal, this figure is displayed as a function of the time by indexing each sample. For the sampling period of 0.2 s, the time axis for this signal varies from 0 to 700 s.

In this figure, the line marked in blue, following the top of this *mountain*, represents the wavelet ridges of the analyzed signal. To associate the instantaneous frequencies to these ridges, we need, first, to compute the scale corresponding to the ridge point, that is, a_{ridge} in Eq. (6.53) at sampling time $b = t_0$. Second, a_{ridge} is transformed to the frequency using Eq. (6.35) in order to obtain the pseudo frequency associated with this scale. This pseudo frequency corresponds to the desired instantaneous frequency at sampling time t_0. Finally, this procedure is repeated in each sampling time to obtain all instantaneous frequencies along time. This procedure will be illustrated with the DR estimation in the following sections.

6.4.3 The discrete wavelet transform and the multiresolution analysis

The CWT, just as the STFT, transforms one-dimensional information contained in a signal into a two-dimensional plane. This means that there exists redundant information contained in the time-scale plane and that it is possible to get a minimal representation of this plane. The best sampling of the time-scale plane is determined by the coefficients $CWT_x(a,b)$ that permit a perfect reconstruction of the signal $x(t)$. This perfect reconstruction is obtained by setting the values:

$$a = 2^j \quad b = k2^j \quad k, j \in \mathbb{Z} \tag{6.55}$$

This sampling creates a plane called dyadic and introduces the discrete wavelet transform (DWT) defined by:

$$DWT_x(j,k) = CWT\left(2^j, k2^j\right) \quad k, j \in \mathbb{Z} \tag{6.56}$$

In addition, the functions $\psi_{j,k}$ become a wavelet basis (not necessarily orthonormal). Construction of these discrete bases, mainly orthonormal, are based on the theory of multiresolution analysis (MRA) introduced by Mallat (Mallat, 1989). This theory indicates that a signal can be decomposed in an *approximation* signal plus a *detail* signal. The approximation signal can be decomposed again in a new coarse-approximation signal and another detail signal. This procedure is shown in Fig. 6.23. The MRA decomposes the signal into approximations $\boldsymbol{a}$ and details $\boldsymbol{d}$. The approximations are smooth versions of the signal and the details contain information about ruptures and discontinuities.

The exact definition of the MRA is given by Mallat (1998): A sequence $\{\mathbf{V}_j\}_{j\in\mathbb{Z}}$ of closed subspaces of $\mathbf{L^2}(\mathbb{R})$ is a multiresolution analysis if the following properties are satisfied:

- $\forall (j,k) \in \mathbb{Z}^2, \quad x(t) \in \mathbf{V}_j \Leftrightarrow x(t - 2^j k) \in \mathbf{V}_j$
- $\forall j \in \mathbb{Z}, \quad \mathbf{V}_{j+1} \subset \mathbf{V}_j$

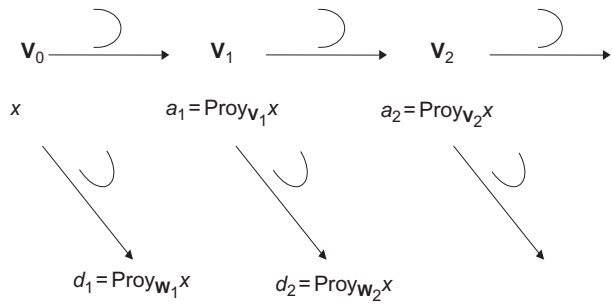

Fig. 6.23 The MRA: details and approximations. The embedded spaces concept.

- $\forall j \in \mathbb{Z},\ \ x(t) \in \mathbf{V}_j \Leftrightarrow x\left(\frac{t}{2}\right) \in \mathbf{V}_{j+1}$
- $\lim_{j \to +\infty} \mathbf{V}_j = \cap_{j=-\infty}^{+\infty} \mathbf{V}_j = \{0\}$
- $\lim_{j \to +\infty} \mathbf{V}_j = \text{Closure}\left(\cup_{j=-\infty}^{+\infty} \mathbf{V}_j\right) = \mathbf{L}^2(\mathbb{R})$
- There exist θ, such that $\{\theta(t-n)\}_{n \in \mathbb{Z}}$ is a Riesz basis of $\mathbf{V}_0$

One of the most important aspects of the MRA is that the details correspond to the DWT. It means that the decomposed signal at different scales $\boldsymbol{L}$, by the MRA, contains in the details the necessary information to determine important transient features present in the signal behavior. In addition, MRA can be linked with orthogonal digital filters that permit MRA to be implemented using a fast algorithm. This implementation is shown in Fig. 6.24, where g and h correspond to digital low-pass and high-pass filters, respectively.

To understand the concept of the MRA, we apply directly this filter bank (Fig. 6.24) on the real instability event presented before. The number of levels (10) in this

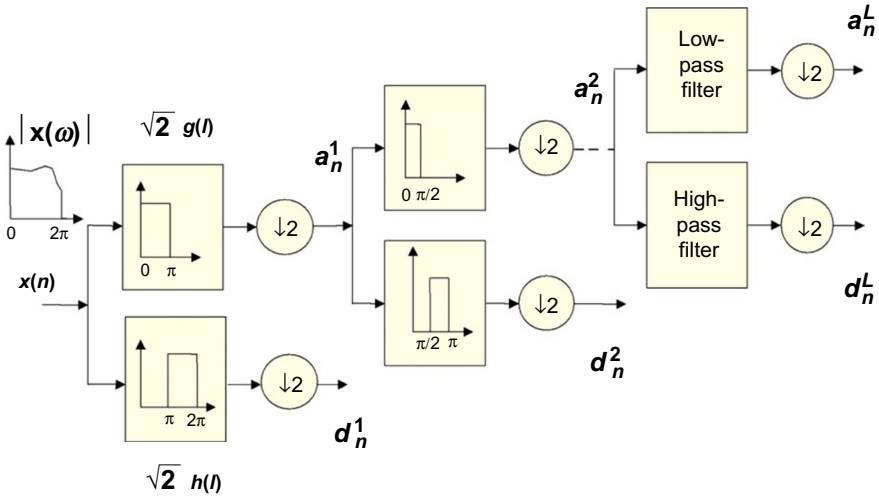

Fig. 6.24 The MRA viewed as a decimated bank filter.

decomposition is set considering the need to obtain a clear behavior in the trend of the analyzed signal. We use again, as in CWT, a Coiflet 2 wavelet.

Two aspects of this analysis should be pointed out:

- First, the detail coefficients become large when the correlation between the signal and the mother wavelet increases. Larger coefficients are obtained at decomposition level 3 (d3) in Fig. 6.25. Generally, a periodic behavior is present in these signals. For this case, from the zoom shown in Fig. 6.26, this behavior is clearly observed as it is possible to detect the evolution of the transient between 368 and 640 s, which corresponds to the beginning and the ending of the event, respectively. Periodicity measured in this signal gives a frequency of 0.521 Hz that represents the same frequency obtained before. Thus, we have a real fast alternative to analyze this kind of signal.
- Second, the *approximation* signal clearly shows the low-pass behavior presented in the signal. This behavior represents the trend of the signal that can be estimated by analyzing the approximations, principally at the last levels.

6.4.4 Wavelets and the decay ratio estimation

Autoregressive methods are used in stability monitoring to estimate the stability parameters, as well as the frequency and decay ratio. They make the assumption that the measured signal is stationary. In normal operation, the signals of a BWR are nonstationary. Because of this, several authors have proposed alternative methodologies adapted for nonstationary signals (Navarro-Esbrí et al., 2003). *Wavelets* is a linear theory but does not need signal stationarity to proceed. To obtain the relationship between CWT or MRA analysis with the stability parameter DR of a BWR, we need to consider the linear model of a BWR, presented in Chapter 5. The impulse response of a simple case of a single degree-of-freedom system is given by:

$$h(t) = A_0 e^{-\zeta\omega_n t} \cos\left(\sqrt{1-\zeta^2}\omega_n t + \theta\right) \tag{6.57}$$

where ω_n is the natural frequency, A_0 is the residue magnitude, and ζ is the damping ratio. Here the oscillation term is represented by an oscillating wave and the damping by the exponentially decaying envelope. It is well known that in order to obtain the dissipative mechanism (damping), the envelope must be analyzed. From the system given by Eq. (6.57), we define the envelope function as:

$$A(t) = A_0 e^{-\zeta\omega_n t} \tag{6.58}$$

Applying a simple calculation, we obtain:

$$\ln(A(t)) = -\zeta\omega_n t + \ln(A_0) \tag{6.59}$$

From Eqs. (6.58), (6.59), it is easy to observe that these expressions correspond to the real part, $x(t)$, for the analytic representation given in Eq. (6.41). Therefore, the theory of wavelet ridges is a well-suited approach to estimate the natural frequencies

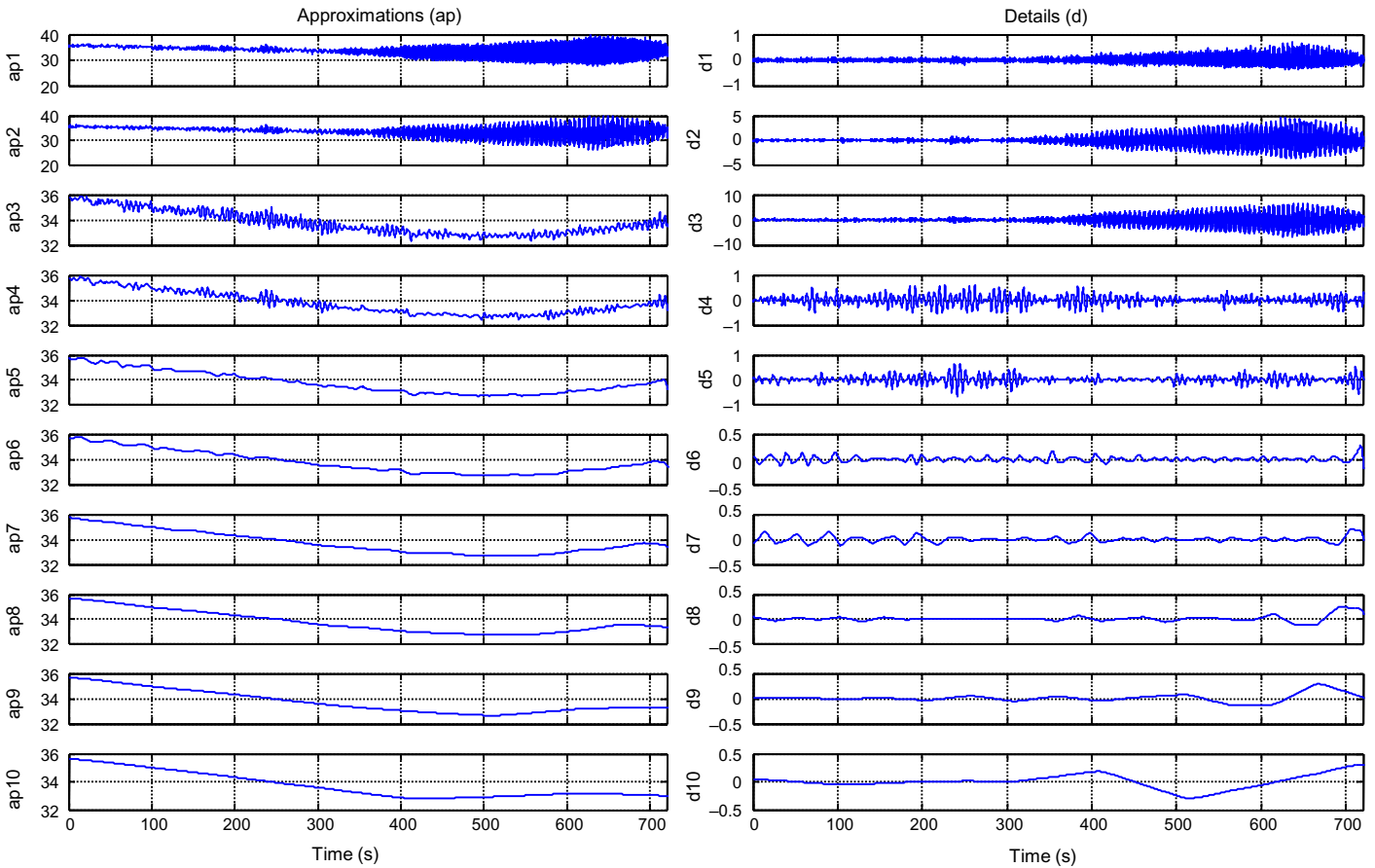

Fig. 6.25 The MRA on a real instability event. Decomposition in 10 levels: on the left side are the *approximations* and on the right side are the *details*.

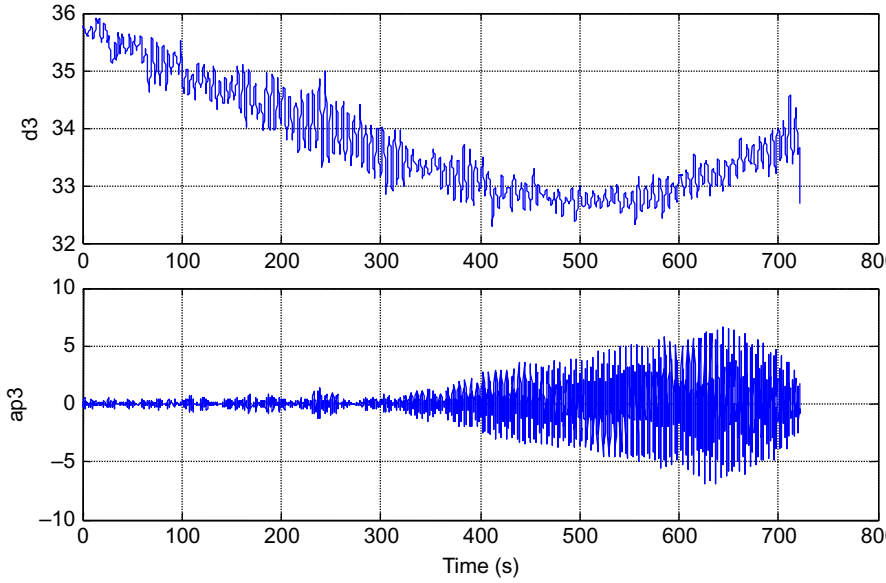

Fig. 6.26 Zoom on the decomposition at level 3.

(the instantaneous frequencies in the analytic representation) and the damping ratio. From Eq. (6.59), we can observe that the damping ratio ζ can be estimated from the slope of the straight envelope line $A(t)$ plotted on a semilogarithmic scale.

6.4.4.1 Decay ratio estimation using the complex Morlet wavelet

If the damping ζ is less than the term k/m, the solution of the system can be established as:

$$x(t) = A(t)e^{\pm j\omega_n\sqrt{1-\zeta^2}t} = A(t)e^{j\phi(t)} \tag{6.60}$$

This solution is an analytic signal in which the envelope $A(t)$ varies slowly. Based on studies developed by Carmona (Carmona, Hwang, & Torresani, 1997) and Staszewski (Staszewski, 1997) about wavelet ridges theory, we can estimate the damping ratio from the wavelet ridge using an analytic wavelet, a complex Morlet wavelet. For this, we use the approximation of the CWT established in Todorovska (2001):

$$CWT_x(a,b) \approx A(b)\hat{\Psi}^*\left(a\dot{\phi}(b)\right)e^{j\phi(b)} + O\left(|\dot{A}|, |\ddot{\phi}|\right) \tag{6.61}$$

where $\hat{\Psi}^*$ is the complex conjugate of the Fourier transform of the complex Morlet wavelet given in Eq. (6.40). The modulus of Eq. (6.61) is given by:

$$|CWT_x(a,b)| \approx A(b)\left|\hat{\Psi}^*\left(a\dot{\phi}(b)\right)\right| \tag{6.62}$$

for a specific value a_0; from Eqs. (6.60)–(6.62), this modulus becomes:

$$|CWT_x(a_0,b)| \approx A_0(b)e^{-\zeta\omega_n b}\left|\hat{\Psi}^*\left(\pm ja_0\omega_n\sqrt{1-\zeta^2}\right)\right| \tag{6.63}$$

by the application of a natural logarithm, we obtain:

$$\ln|CWT_x(a_0,b)| \approx -\zeta\omega_n b + \ln\left(A_0\left|\hat{\Psi}^*\left(\pm ja_0\omega_n\sqrt{1-\zeta^2}\right)\right|\right) \tag{6.64}$$

Therefore, the damping ratio ζcan be estimated, for a specific value a_0, from the straight line obtained from Eq. (6.64) plotted on a semilogarithm scale. The relationship between Eqs. (6.59) and (6.64) is revealed. It is clear that these expressions are similar. To associate the wavelet ridges with the estimation of the damping ratio ζ, we must consider results obtained before that show that the wavelet ridges can be obtained from the modulus *maxima* of the CWT of the analyzed signal $x(t)$. Based on this fact, by estimating first the wavelet ridges of $x(t)$ at the stationary points $t_0(a,b)=b$, the instantaneous frequencies ω_{inst} can then be obtained along these ridges (Eq. 6.54). It is not easy to match the concept of instantaneous frequency with the natural frequency ω_n of a dynamic system. However, if we consider that the existing natural frequency is unique, then this frequency can be tracked with the wavelet ridges and treated as instantaneous along time. Finally, the DR is calculated as:

$$\mathrm{DR} = \exp\left(-\frac{2\pi\zeta}{\sqrt{1-\zeta^2}}\right) \tag{6.65}$$

Continuing with the analysis presented previously with a real signal, and taking into account how to estimate now the DR, we can obtain this parameter after calculating the wavelet ridges (Fig. 6.21). After that, we change the scale values associated with these ridges to the instantaneous frequencies (in Hz) using Eq. (6.54). These ridges (instantaneous frequencies) are plotted in the second row of Fig. 6.27. The third row of Fig. 6.27 shows the same wavelet ridges but considers only the *maxima* at every instant of time b. The fourth row shows the natural logarithm of the magnitude of the values of the CWT associated with the ridges. By using Eq. (6.64) we determine the damping along time and with Eq. (6.65) we can finally obtain the DR. The DR is plotted in the last row of Fig. 6.27.

From the results shown in Fig. 6.27, it is clear that we can perfectly determine the resonant frequency of the system. This instant in which the power level increases is marked by the frequency located in the neighborhood of 0.54 Hz. This phenomenon is caused by the lag introduced into the thermal-hydraulic system by the finite speed of propagation of the density perturbation. For high core void fractions, the feedback becomes so strong that it induces oscillations at a frequency of 0.5 Hz, and when this feedback increases the oscillations become more pronounced and an oscillatory instability can be reached. This can be observed after sample 1835 (367 s) in the zoom of Fig. 6.27, presented in Fig. 6.28. This is an indication that the oscillation has started

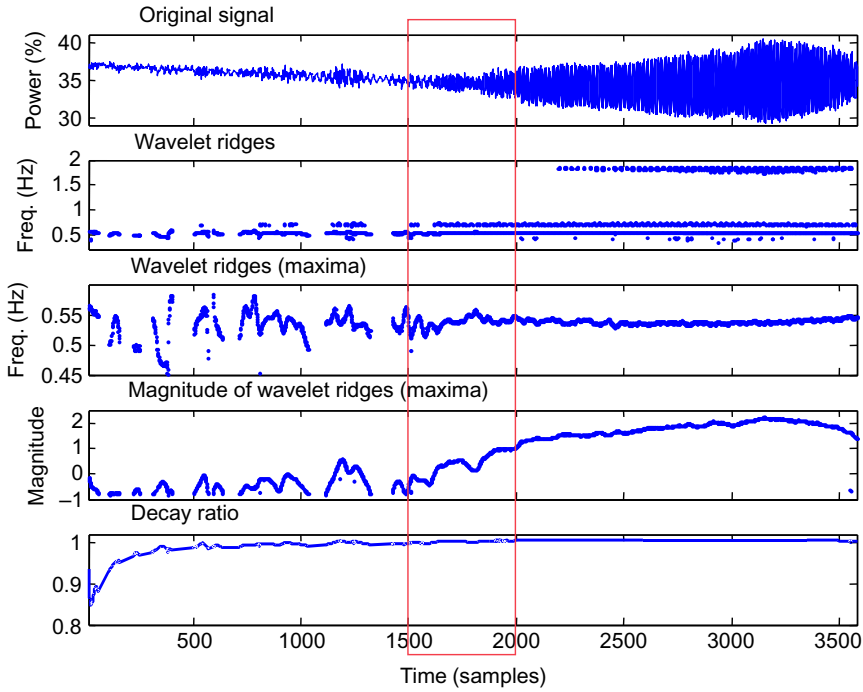

Fig. 6.27 Wavelet ridges and DR estimation for a real instability event in a BWR.

and can be avoided, but the manual action of the reactor operator after 367 s induces a significant increase of the oscillation.

In Figs. 6.27 and 6.28, we can observe that the DR is about 0.8 at the beginning of the event, but increases to a value of about 1.0 during the closure of the control valve, and then reaches a maximum value when the flow control valves were closed to their minimum position (about 350 s, sample 1750). Then, the reactor operator opened the control flow valves in order to damp the oscillations and the DR decreases just before the scram of the reactor.

Sunde and Pázsit (Sunde & Pázsit, 2007) proposed an original work using the wavelet transform in combination with the autocorrelation function. They consider the dynamic behavior of a BWR core in the stable region described as a second-order system. They obtain, based on this model, the autocorrelation function of the system output (the flux fluctuations in the core, in this case) and then they apply the CWT using a complex wavelet to this autocorrelation function (expressed as a function of the damping ratio and the resonant frequency of the system, in this case around 0.5 Hz). Hence, they obtain the ridges of the CWT associated with this autocorrelation function. The decay ratio is finally obtained from these ridges and the resonant frequency.

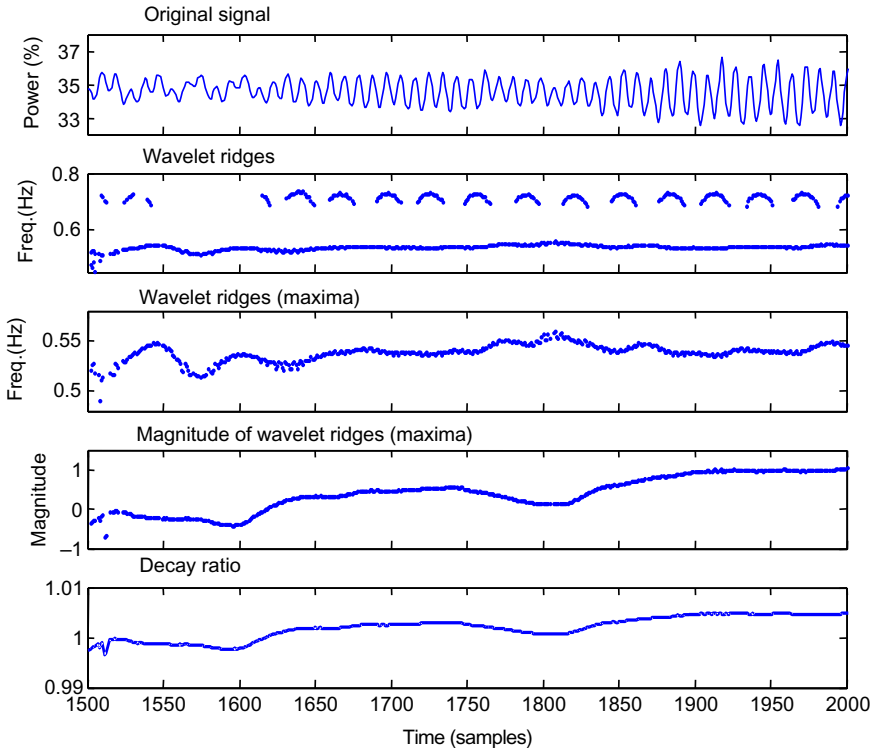

Fig. 6.28 Wavelet ridges and DR estimation for a real instability event in a BWR (zoom).

6.4.4.2 Methodology to estimate the DR using wavelets

Based on the theoretical elements and practical aspects about wavelets theory, presented in previous sections, we propose a methodology to analyze stability events in a BWR.

6.5 Application of the multiresolution analysis

Multiresolution analysis allows for a fast implementation of the DWT. Exactly as in CWT, the choice of the wavelet determines the performance of this method. Several wavelets must be tested to obtain optimum results. Daubechies and Coiflets wavelets are good candidates because they have good properties, such as being regular and compact in time; nevertheless, others wavelets can be used. The signal features that can be detected at different decomposition levels are important ruptures, signal trend, and important frequencies. To determinate these features, sometimes it is necessary to perform a decomposition in *many* levels. The signal trend is obtained by analyzing the low-pass behavior contained in the signal. This behavior is shown in the approximation coefficients in all decomposition levels, however, the best results are obtained in

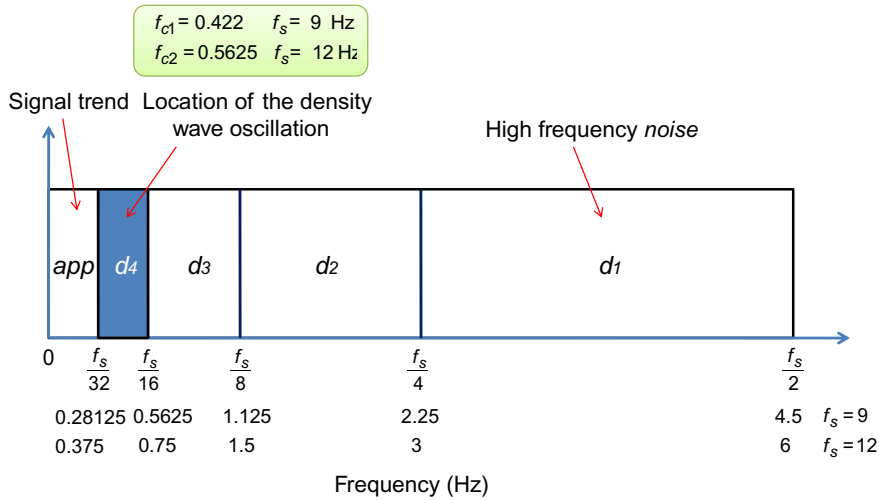

Fig. 6.29 The dyadic filter bank with MRA. A practical point of view to analyze BWR signals.

the deepest decomposition levels. Features, such as important frequencies, discontinuities, and transients, can be detected with analysis at different levels of the detail coefficients corresponding to DWT. The important frequencies of the signal are clearly identified when the detail coefficients show oscillations (the oscillation due to a density wave for instance) around these frequencies. Transients can be detected as a path traced by the maximum contained in the detail coefficients through different levels in the signal decomposition. Good detection of transients depends on the property of wavelet regularity.

The levels number in MRA is very important to track the oscillation due to the density wave around 0.5 Hz. Indeed, in Fig. 6.29, we show how the dyadic filter bank, implemented by the MRA, works. In this figure, we can observe that if we choose wrongly the sampling frequency f_s, the tracked mode around 0.5 Hz can be dismissed (attenuated by the transition bands of these filters). To enhance the detection, this mode must be placed around the central frequency of the right band. For instance, in Fig. 6.29, we placed two different sampling frequencies to illustrate this situation. In the first case ($f_s = 9\,\mathrm{Hz}$), the tracked mode lies practically in the transition band of the second and third levels. In the second case ($f_s = 12\,\mathrm{Hz}$), the oscillation mode lies practically in the central frequency of the third band and becomes a good choice.

Another important thing about MRA is that this decomposition can be used as a first denoising of the analyzed signal before processing to estimate the DR. For this, observing again Fig. 6.29, the details from the first level correspond, in general, to the components associated with a *high-frequency* noise. To suppress this noise, we modify these detail coefficients using a criterion (hard or soft) and we reconstruct the analyzed signal with these detail coefficients, suppressed or modified by this criterion. Based on this recommendation, it is important to mention that Tambouratzis and Antonopoulos-Domis (Antonopoulos-Domis & Tambouratzis, 1998) presented a

methodology based on MRA with a selective coefficient removal to estimate the system parameters during transient operation. The wavelet analysis was used to separate the signal into two parts: (1) the expectation value, and (2) nonstationary noisy signal. After this decomposition, the inverse wavelet transform allows the estimation of the transient part of the signal. These authors implemented an application for BWR stability using numerical experiments, that is, real BWR signals were not used.

6.6 Application of the continuous wavelet transform

CWT gives information about ruptures, discontinuities, and fractal behavior that are present in the analyzed signal. To detect these important features in the signal, the choice of the mother wavelet is crucial. Indeed, CWT coefficients become large when the correlation between the signal and the selected wavelet is relevant. With this choice, the signal must be analyzed at several scales. The choice of these scales is dependent on the signal because sometimes the analysis is more revealing at small scales and in other cases at large scales. Nevertheless, a global analysis at several scales (small and large) is necessary. In CWT, discontinuities are shown as a *cone* with its peak at the time of the discontinuity. Fractal behavior is revealed by a repeated pattern along time.

Based on these remarks, we can establish the next methodology to estimate the DR as follows:

Step 1. Perform a denoising of the BWR signal using the MRA. The levels number must be carefully chosen, based on recommendation 1.
Step 2. Track the oscillation due to the density wave, around 0.5 Hz, in the corresponding detail level.
Step 3. Obtain the wavelet ridges from the modulus *maxima* of the CWT of the denoised signal using a complex wavelet, such as the *Morlet*.
Step 4. Compute the instantaneous frequencies along these ridges.
Step 5. Determine the damping ratio based on these instantaneous frequencies.
Step 6. Estimate the DR based on the damping ratio.

This methodology is resumed in Fig. 6.30.

6.7 Other linear methods

Throughout this chapter, we have presented the most used classical linear methods, and some not so classic, for the estimation of the DR. Contributions to the estimation of this stability indicator in BWRs have been manifold over the past two decades. Most of the proposals are framed in these classical methods, always delineated around the autocorrelation function and the PSD and their relationship with the second-order linear model of a BWR.

In this last section, we include a brief description of other linear methods that have been applied for DR estimation. We consider that the explanations given in the

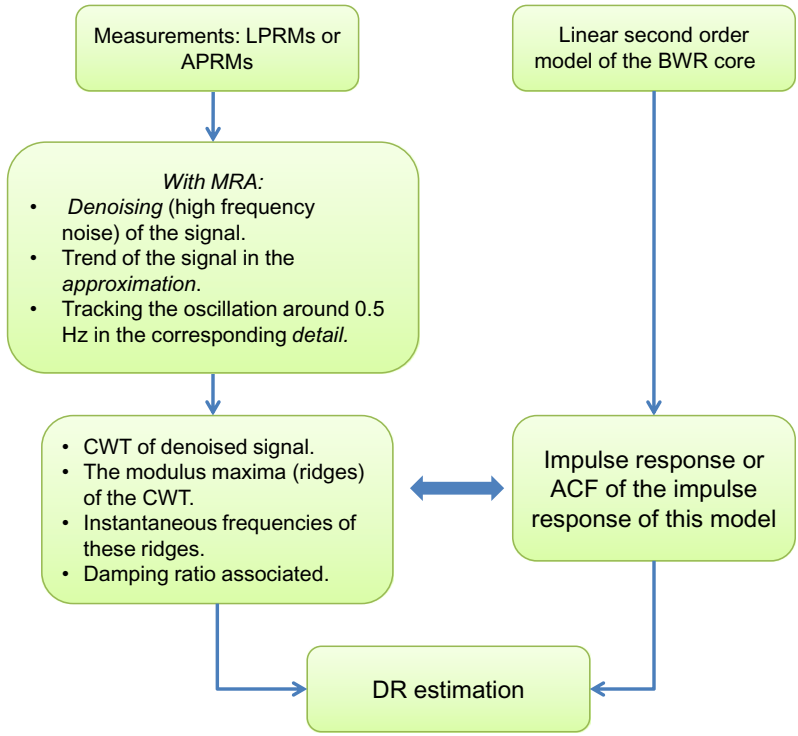

Fig. 6.30 DR estimation using wavelets, a guide.

previous sections contribute enough to lead (or motivate) the reader to a greater depth of study in the matter, if considered pertinent.

6.7.1 The ARMA model

This model is the generalization of the AR model (Eq. 6.13) and is established as:

$$x(n) = -\sum_{k=1}^{p} a_k x(n-k) + \sum_{l=0}^{q} b_l v(n) \tag{6.66}$$

Now, the model considers the $q+1$ past values of the driven input (the white Gaussian noise, explained before) giving a rational transfer function:

$$H(z) = \frac{X(z)}{E(z)} = \frac{B(z)}{A(z)} = \frac{\sum_{l=0}^{q} b_l z^{-k}}{1 + \sum_{k=1}^{p} a_k z^{-k}} \tag{6.67}$$

The coefficients b_l are known as the moving average (MA) parameters. Like the AR model, we can obtain the frequency response of this model and link it with the second-order linear model of a BWR to estimate the DR. The Wold decomposition theorem (Wold, 1954) relates the ARMA, MA, and AR models, indicating that any stationary ARMA or MA process of finite variance can be modeled by an AR model of a possible finite order, that is, we can approximate an ARMA model with an AR model using a higher order. The advantage of using an AR model instead of an ARMA resides in the use of linear equations to estimate its model parameters.

6.7.2 Time-frequency representations

The main objective of time-frequency analysis (TFA) is to describe how the energy of a signal is jointly distributed in the time-frequency domain. This is an ill-posed problem because a bidimensional representation must be somewhat generated from a one-dimensional signal. In the digital domain, it can be argued that the number of unknowns is greater that the number of *knowns* represented by the signal points. Therefore, there are many potential solutions (time-frequency representations, TFR) for any given signal, but not all of them are nontrivial and useful. In order to accurately represent time varying spectra, the TFA problem must be constrained to eliminate the trivial and useless solutions. The constraints are derived from the properties that a TFR ideally should meet (Cohen, 1995).

It is worth mentioning that not all TFRs meet all these properties and nor is necessary at all. For instance, the most used and well-known TFR is the *spectrogram* or STFT (presented before), which does not satisfy the *marginals property*. Also, most TFRs do take negative values despite the fact that TFRs are supposed to be densities. Any TFR can be uniquely expressed in terms of the general class equation given by (Cohen, 1995):

$$C_x(t,\omega;\phi) = \iiint x^*(u-\tau/2)x(u+\tau/2)\phi(\theta,\tau;s)\exp(-j\theta t - j\tau\omega + j\theta u)du d\tau d\theta \tag{6.68}$$

where $x(t)s(t)$ is any square integrable signal, and $\phi(\theta,\tau;s)$ is the TFR kernel, which can depend on $x(t)$, * represents a complex conjugate. Suffice it to say that the desired TFR properties are translated into kernel constrictions, making TFR design equivalent to kernel design.

There have been previous research efforts on how to estimate the DR of BWRs using TFRs (Torres-Fernández, Prieto-Guerrero, & Espinosa-Paredes, 2009; Torres-Fernández, Espinosa-Paredes, & Prieto-Guerrero, 2012). The research in Torres-Fernández et al. (2009) deals with estimating the DR of BWRs using bilinear TFRs, which, conceptually speaking, differ greatly from the TSRs employed in Torres-Fernández et al. (2012), in which a method based on time scale representations (TSRs) to estimate the decay ratio (DR) is presented. However, this latter methodology is based on the deduction of a generalized class equation for TSRs, which is

similarly derived as the time-frequency general class equation in time-frequency analysis, and the results from these two different methodologies converge with each other. This convergence is due to the common math background shared by these two different methodologies. Indeed, there is a link between bilinear TFRs and TSRs in which the latter can be obtained from the former by a change of variables in which frequency is substituted by the inverse of the scale times a constant factor. Another similarity between both works is the estimation of *instantaneous* decay ratios (IDR) as opposed to a classic decay ratio that is constant over the entire analysis window. The TFR (or TSR) is obtained considering the impulse response of a linear second-order model for a BWR.

6.7.3 Singular value decomposition-based methods

The theory of singular value decomposition (SVD) was introduced in 1981 by Kumaresan (Kumaresan & Tufts, 1981) for the parametric spectral analysis and corresponds to a generalization of the eigenvalues decomposition theory of a rectangular matrix. That is, consider a matrix $\mathbf{A}$ of size $m \times n$ with $m \geq n$, then there exist two orthogonal matrices $\mathbf{U}$, $\mathbf{V}$ of size $m \times m$ and $n \times n$, respectively, and a quasidiagonal matrix $\mathbf{Q}$ of size $m \times n$ satisfying:

$$\mathbf{A} = \mathbf{U}\mathbf{Q}\mathbf{V}^t \tag{6.69}$$

with $\mathbf{U} = [\mathbf{u}_1 \ \ \mathbf{u}_2 \ \ \ldots \mathbf{u}_m]$ and $\mathbf{V} = [\mathbf{v}_1 \ \ \mathbf{v}_2 \ \ \ldots \mathbf{v}_n]$ where $\mathbf{u}_i$ and $\mathbf{v}_i$ are the singular vectors of $\mathbf{A}$, and

$$\mathbf{Q} = \begin{bmatrix} \sigma_1 & & & \\ & \sigma_2 & & \\ & & \ddots & \\ & & & \sigma_n \\ \ldots & 0 & 0 & \ldots \end{bmatrix} \tag{6.70}$$

where σ_i are the singular values of $\mathbf{A}$.

In the case of an AR model, we need to resolve a linear equations system, based on the autocorrelation matrix, to find the corresponding model parameters (Eq. 6.18):

$$\mathbf{R}'\mathbf{a}' = 0 \ \text{ with } \mathbf{R}' = [\mathbf{r}|\mathbf{R}] \tag{6.71}$$

Using SVD, the idea is to eliminate the noise present in this autocorrelation matrix. It was demonstrated (Kumaresan & Tufts, 1982) that for a signal composed of M sinusoids with noise, if we choose an order $p \geq 2M$, the first $2M$ greatest singular values correspond to the signal and the other ones represent the noise. Based on this fact, we can perform a separation in two subspaces, the signal space and the noise space:

$$\mathbf{Q} = \mathbf{Q}_s + \mathbf{Q}_n \tag{6.72}$$

with $\mathbf{Q}_s$ containing the singular values of the signal and $\mathbf{Q}_n$ those of noise. In the case of the autocorrelation matrix, we have:

$$\mathbf{R}' = \mathbf{U}\mathbf{Q}\mathbf{V}^t = \mathbf{U}\mathbf{Q}_s\mathbf{V}^t + \mathbf{U}\mathbf{Q}_n\mathbf{V}^t = \mathbf{R}'_s + \mathbf{R}'_n \tag{6.73}$$

If we replace $\mathbf{R}^{'}$ by $\mathbf{R}^{'}_s$, we eliminate the noise, having for effect to enhance the estimation of parameters a_k. Based on these ideas, some efforts have been made to enhance the estimation of the DR (Navarro-Esbrí, Verdú, Ginestar, & Muñoz-Cobo, 1998; Tsuji & Shimazu, 2005).

This technique gives the effective number of sinusoidal components from $\mathbf{R}^{'}$ and permits us to enhance the spectral estimation for a higher order. However, in practice this technique is efficient, but its computational complexity is important in comparison with the Levinson-Durbin algorithm. Besides, the singular values separation is disturbed by the signal-to-noise ratio, the ratio between the amplitudes of the sinusoids and the proximity between the signal frequencies.